MODIFIED LAGRANGIAN-MEAN PERSPECTIVE OF ANNULAR MODE VARIABILITY

A Thesis

Presented to the Faculty of the Graduate School

of Cornell University

In Partial Fulfillment of the Requirements for the Degree of

Master of Science

by

David A. Burrows

January 2014

ABSTRACT

The leading mode of extratropical variability or annular mode is characterized as a meridional seesaw of mass between middle and high latitudes or equivalently, a barotropic dipole in the zonal wind anomaly field. With an understanding of the spatial structure of the annular mode variability, focus has shifted to the eddy-zonal flow interaction or Rossby wave breaking that leads to the persistence of the zonal wind anomalies. Much insight has been gained from the conventional relationship between the zonal-mean flow and eddy fluxes, and the resulting mechanisms often involve eddies of different frequencies or barotropic versus baroclinic processes.

Here a new perspective of the annular mode variability is presented in the Modified Lagrangian-Mean (MLM) formalism of a quasi-geostrophic (QG) and absolute vorticity model. By applying the MLM to the QG potential vorticity (PV) tendency budget, a closure equation for annular mode variability or eddy vorticity flux can be obtained. The eddy vorticity flux closure model can be described by a simple diffusive equation with the eddy fluxes absorbed in the MLM. A similar diffusive equation is obtained using absolute vorticity but with a redefinition of the wave type and wave source. Instead of a QG PV, baroclinic wave source, absolute vorticity provides a horizontally, divergent source of waves which are important for wave propagation, wave breaking, and annular mode variability.

These formalisms are applied to a baroclinic eddy lifecycle and annular mode variability in an idealized model. It is shown that the shift of a zonal jet during an eddy life cycle can be attributed to horizontal wave tendency, whereas its persistence is concurrent with small-scale dissipation associated with Rossby wave breaking. Furthermore, analysis of annular modes in the idealized model suggests that the wave activity associated with the annular mode variability

is short-lived, and that the persistence of the annular mode may be attributed to the eddy source and diffusion of the eddy vorticity flux also associated with Rossby wave breaking.

BIOGRAPHICAL SKETCH

David A. Burrows graduated magna cum laude with a Bachelor of Arts in mathematics and a minor in geography from Castleton State College. He continued his education at Metropolitan State College of Denver studying atmospheric science. David is now completing his Master of Science degree in atmospheric science and will continue at Cornell University to obtain his doctorate degree.

For supporting me from day one, I dedicate this thesis to my parents.

ACKNOWLEDGMENTS

I would like to acknowledge the support from my advisor, Dr. Gang Chen, whose weekly meetings provided the necessary guidance to complete this research project. I also acknowledge other members of my special committee, Drs. Stephen Colucci and Peter Diamesis, who provided support for finalizing this manuscript as well as generalizing this manuscript for a much broader audience. Doctors Gang Chen and Lantao Sun are also acknowledged for providing data from the GFDL's spectral core model. Finally, I acknowledge support from my entire research group who allowed me to present this material multiple times throughout its development.

TABLE OF CONTENTS

LIST OF FIGURES

CHAPTER 1

INTRODUCTION

The zonal-mean state of the atmosphere has received much attention dating back to the mid-twentieth century consisting of an eddy driven zonal jet. Initial descriptions of the leading mode of extratropical variability include a meridional seesaw of mass or pressure anomaly dipole and equivalently, a zonal-mean zonal wind dipole (Rossby 1939; Willett 1948; Namias 1950). This is the pattern coined by Thompson and Wallace (2000) as the annular modes. The spatial attributes of the annular modes were well described for both hemispheres in the following decades to include meridional dipoles in sea-level pressure (Lorenz 1967; Kutzbach 1970), zonal wind (e.g. Webster and Keller 1975; Trenberth 1979), and geopotential height (Rogers and van Loon 1982). These patterns also extend into the stratosphere (Baldwin et al. 1994). Another spatially significant attribute is that forcing mechanisms on climatic timescales such as greenhouse gasses (Fyfe and Saenko 2006), ozone depletion and recovery (e.g. Thompson and Solomon 2002), and solar variability (Haigh et al. 2005) project strongly onto the annular mode structure. The temporal attributes present a more complicated picture with low- and high-frequency eddies interacting to produce longer time scale variability than can be explained by frictional dissipation alone (Lorenz and Hartmann 2001). Whereas the annular modes are sensitive to external forcing mechanisms such as ozone and GHG, Limpasuvan and Hartmann (1999) and DeWeaver and Nigam (2000a) have shown that annular mode variability can be sustained independent of these forcing mechanisms and solely rely on internally driven, atmospheric dynamics.

Annular mode variability requires excessive amounts of mass transfer in order to shift and accelerate jets. Atmospheric waves provide a large source of mass transfer, and the breaking of these waves is crucial to the advancement of short term weather forecasting and seasonal to intraseasonal variability in the midlatitudes (McIntyre and Palmer 1983). These wave breaking characteristics coincide strongly with the North Atlantic Oscillation (NAO) which is a regional pattern, remarkably similar to the annular modes (Benedict et al. 2004; Franzke et al. 2004). Synoptic waves predominately break anticyclonically for the high index and cyclonically for the low index states of the annular mode, shifting the zonal jet poleward and equatorward, respectively. Wave breaking and its irreversible characteristics present many difficulties in describing interactions with the mean flow. Through the use of refractive indices, critical layer theory, small-amplitude wave activity (Vallis 2006) and other variables, linear theory has provided much insight into wave propagation which links directly to momentum and mass fluxes (Edmon et al. 1980). Recently, a finite-amplitude formalism for wave activity was presented that allows for a direct relationship to be drawn between the wave tendency and the zonal-mean zonal wind tendency (Nakamura and Zhu 2010), not realizable in the small-amplitude limit. Finite-amplitude wave activity provides a momentum flux budget which can be analyzed for contributions to eddy-mean and wave-mean flow interactions.

Debate continues as to the mechanisms responsible for eddy-mean flow feedback and the persistence of the zonal wind anomaly including two main categories, barotropic and baroclinic. A barotropic mechanism depends on upper-level wave propagation and has been analyzed extensively using linear wave theory (Simmons and Hoskins 1978; Hartmann and Zuercher 1998; Chen and Zurita-Gotor 2008). In a momentum budget analysis, Lorenz and Hartmann (2001) showed how a burst eddy-momentum flux acts rapidly to alter the mean flow. This new

mean state is then reinforced with more momentum that is independent of the initial burst. This feedback produced decorrelation time scales that constituted a positive feedback between eddies and the mean flow. The importance of a barotropic mechanism is gleamed in recent studies that indicates the latitudinal dependence of the eddy feedback which may help to explain zonal index persistence biases in models (Barnes and Hartmann 2010; Barnes et al. 2010; Arakelian and Codron 2012; Kidston and Vallis 2012). This study will implement absolute vorticity waves as the barotropic mechanism aiding to flux momentum directly into the jet core.

A baroclinic mechanism relies on low-level baroclinicity that provides a source region for waves into the upper troposphere. If the source region is meridionally concurrent with the zonal wind anomaly, wave fluxes out of the jet will provide the momentum fluxes necessary to accelerate or shift a zonal jet. If a source region is meridionally displaced from the jet region, the waves will flux into the jet and remove momentum. Lorenz and Hartmann (2001) showed that accompanying the zonal wind anomaly is a similar shift in the maximum lower-level baroclinicity, providing a baroclinic feedback. Other baroclinic mechanisms have been proposed including enhanced surface friction, which induces low-level vertical shear or enhanced baroclinicity (Robinson 2000). This was demonstrated by directly increasing the low-level vertical shear, but consistent results were not found when increasing surface drag parameters themselves (Chen and Plumb 2009). Also, an indirect residual meridional circulation induced by a maximum Eliassen-Palm (EP) flux convergence at the jet core again enhances low-level baroclinicity (Robinson 2006; Gerber and Vallis 2007). Most likely, it is not solely one mechanism providing the feedback but more likely a combination of interacting positive and negative feedbacks as demonstrated by Zurita-Gotor et al. (2014). Whereas Barnes et al. (2010) and Barnes and Hartmann (2011) showed the source of baroclinic waves does not necessarily

need to shift in order to produce realistic zonal index persistence timescales, this study will implement QG PV waves as a baroclinic source that is free to provide feedback support.

The goal of this study is to examine two closure models for momentum flux convergence budgets through an eddy lifecycle experiment and an idealized model run. Sardeshmukh and Hoskins (1988) presented the framework for absolute vorticity conservation, while Nakamura and Zhu (2010) set the framework for QG PV conservation. Through the use of an eddy operator introduced in Nakamura and Zhu (2010), QG PV and absolute vorticity tendency budgets can each provide a closure for eddy momentum flux convergence. Eddy momentum convergence or equivalently eddy vorticity flux can be decomposed into three terms: a negative wave activity tendency term, a wave source term, and a small-scale dissipation term. Besides defining waves using different vorticity arrangements, there is also a redefinition of wave source. The familiar heat flux convergence source provides QG PV waves (Edmon et al. 1980), while the Rossby wave source term in Sardeshmukh and Hoskins (1988), with the use of the eddy operator, becomes a horizontally, divergent vorticity flux that provides the source of absolute vorticity waves. In this sense, the source terms for QG PV and absolute vorticity waves act as vertical and horizontal source of waves, respectively. The main objective is to assess the validity of these two closures, compare the barotropic and baroclinic dynamics associated with both definitions of vorticity, and provide insight into the mechanisms governing zonal wind shift and persistence.

To facilitate such a study, an eddy lifecycle experiment and a run from the Geophysical Fluid Dynamics Laboratory (GFDL) steady state model will be used. Simmons and Hoskins (1980) first noted how a perturbation introduced into a baroclinic jet may follow two distinct lifecycles dubbed by Thorncroft et al. (1993) as lifecycle-1 (LC1) and lifecycle-2 (LC2). The persistence of a poleward shifting zonal jet in LC1 underlies the importance for predictability.

Hartmann and Zuercher (1998) showed that a slight change in the zonal-mean barotropic shear marks transitions from LC1 to LC2. This study will use the same transition mechanism, barotropic shear, and specifically look at the transition case studied in Solomon et al. (2012).

The following chapter reviews the spatial and temporal attributes of annular mode variability as well as its importance for climate projections. The third chapter reviews the QG PV closure model and presents the absolute vorticity closure model both mathematically and conceptually. The fourth chapter details the simplified atmospheric model and steady state model and diagnostics used in this study. The results for both models are presented in chapter five. Concluding remarks are in chapter six, and future work is in chapter seven. Additionally, Appendix A describes the details of using the MLM, and Appendix B provides a detailed explanation of how wave breaking is calculated.

CHAPTER 2

Annular Modes: Observations and Projections

With such a huge extent of research contributing to annular mode variability, this section will provides a brief history followed by the importance of the annular modes in future climate projections. As mentioned in the introduction, the annular mode, spatially, represents a shift of the eddy-driven midlatitude jet. In observations with respect to the climatological jet position, the jet is shown to accelerate in its poleward-shifted position, high index state, and decelerate in its equatorward-shifted position, low index state. This feature represents a meridional dipole in pressure anomalies that in the high index state provide low heights over the poles with high heights surrounding it in the midlatitudes (e.g. Rossby 1939; Willett 1948; Namias 1950; Lorenz 1967; Kutzbach 1970; Webster and Keller 1975; Trenberth 1979; Rogers and van Loon 1982; Thompson and Wallace 2000a). This high and low index state also manifests itself at the regional scale in the typical storm track regions over the ocean basins. An example of the North Atlantic Oscillation was presented in Woolings et al. (2010). High index composites show a zonal jet that is shifted north of its climatological position impacting regional weather over the eastern Canada and United States border and northern Europe. These smaller scale annular mode features provided a more physically recognizable forcing mechanism to the annular mode large scale signature. Lorenz and Hartmann (2001) determined that the convergence of eddy momentum provided both the regional and global annular mode structure. But the paper also showed that the eddy momentum mechanism was very short-lived whereas the impact on a midlatitude jet shifted extended well beyond the lifetime of the eddy itself. Whereas the forcing mechanism produces power almost equally at all timescales, the annular mode response is a majority low frequency, greater than 20 day, response. This long-term decay provides hope at the use of annular mode variability in weather predictability, on the order of a couple weeks.

With the predictive capability of the annular modes, it is essential to understand the forcing mechanisms as well as the mechanisms that prolong the shift of the jet. But recently, the importance of annular mode variability has truly come to light. Climate projections are extremely important for providing details into how the climate system may respond to certain forcing mechanisms, natural or anthropogenic. It is also extremely important to get the climate projections correct because of the effect it has on global policy making and the welfare of the global population. A natural system that may respond to anthropogenic forcing is the El Nino Southern Oscillation (ENSO) pattern. By projecting a time series associated with the ENSO cycle onto a spatial structure associated with the annular mode, L'Heureux and Thompson (2005) showed that the structure is highly similar to the annular mode structure indicating a poleward-shifted jet. Global warming and the forcing from greenhouse gases project onto the annular mode pattern. Woolings et al. (2010) showed that by doubling the CO_2 on the Earth, the resulting leading mode of variability is an enhanced annular mode response indicating a poleward-shifted jet. Son et al. (2008) showed that with ozone recovery in the Antarctic, the response in the annular modes is an equatorward-shifted jet. With the complexities presented in these global climate models and the physical processes underlying weather and climate prediction, it is essential to fully understand all aspects representing annular mode variability. This paper will therefore examine models and experiments that simplify the dynamics of annular mode variability but that are also consistent with observations of annular mode variability.

CHAPTER 3

Diagnostics

3.1 Mathematical Theory

Consider the linearized barotropic vorticity equation

$$\frac{\partial \zeta'}{\partial t} + \bar{u}\frac{\partial \zeta'}{\partial x} + v'\beta = F + \kappa\nabla^2\zeta' \tag{1}$$

where overbars denote zonal-mean and primes the deviation therefrom, F is a source of eddy vorticity and $\kappa\nabla^2\zeta'$ is the diffusive flux of eddy vorticity. Multiplying (1) by ζ', taking the zonal-mean, and dividing through by β yields the wave activity equation for eddy vorticity flux

$$\overline{v'\zeta'} = -\frac{\partial A_{\zeta'}}{\partial t} + \frac{\overline{\zeta' F'}}{\beta} + \kappa\frac{\overline{\zeta'\nabla^2\zeta'}}{\beta} \tag{2}$$

where $A_{\zeta'} = \frac{\overline{\zeta'^2}}{2\beta}$ defines the small-amplitude form of wave activity (Vallis 2006). Amendments to this linear theory include refractive indices and critical line distribution (Simmons and Hoskins 1978; Hartmann and Zuercher 1998; Chen and Zurita-Gotor 2008; Lorezn 2013a,b). Even though these quantities are quite useful for annular mode research (e.g. Lorenz and Hartmann 2001; Zhang et al. 2012), these approximations break down when waves grow beyond a small amplitude, linear limit.

More generally, consider a tendency budget for a quasi-conservative tracer q as

$$\frac{\partial q}{\partial t} + \vec{v}_\psi \cdot \nabla q = \dot{q}_s + \kappa\nabla^2 q \tag{3}$$

where the non-divergent, advecting flow $\vec{v}_\psi$ is defined by the streamfunction ψ as $\vec{v}_\psi = \nabla \times \mathbf{i}\psi$, and $\mathbf{i}$ is the unit vector in the zonal direction, $\kappa\nabla^2 q$ is the diffusive flux of the tracer with diffusion coefficient κ, and $\dot{q}_s$ is any other source or sink of the tracer. The finite-amplitude wave activity budget, following Nakamura and Zhu (2010) (see the derivations from (9) to (25)), can be written as

$$\frac{\partial A_q}{\partial t} + \overline{v_\psi' q'} = \Delta M(\dot{q}_s) + \Delta M(\kappa\nabla^2 q) \tag{4}$$

where A_q is the finite-amplitude wave activity, $\Delta M(\dot{q}_s)$ the wave source, $\Delta M(\kappa\nabla^2 q)$ the diffusive sink. An eddy operator ($\Delta\Sigma$ in the notation of Nakamura and Zhu (2010)) is defined as

$$\Delta M(X) = \frac{1}{2\pi\cos\phi_e}\left(\iint_{q>Q,\phi\le\phi_e(Q)} X dS - \iint_{q\le Q,\phi>\phi_e(Q)} X dS\right) \tag{5}$$

where ϕ_e is the equivalent latitude for the value of Q (Butchart and Remsberg 1986). See Appendix A for a detailed description of how the eddy operator is used. In the absence of sources and sinks of wave activity, the wave activity tendency is balanced by the eddy tracer flux across the latitude ϕ_e

$$\frac{\partial A_q}{\partial t} + \overline{v_\psi' q'} = 0\,. \tag{6}$$

There are two ways to provide the closure associated with the eddy vorticity flux as in (2). The first is to define the tracer through the conservation of QG PV, defined as

$$q_{QG} = 2\Omega\sin\phi + \zeta + f\frac{\partial}{\partial p}\left(\frac{\theta-\Theta}{\partial\Theta/\partial p}\right) \tag{7}$$

where Θ is the hemispherically averaged potential temperature. For adiabatic conditions, the QG PV tendency equation becomes

$$\frac{\partial q_{QG}}{\partial t} + \vec{v}_\psi \cdot \nabla q_{QG} = \kappa \nabla^2 q_{QG} \tag{8}$$

and following (4), the wave activity equation becomes

$$\frac{\partial A_{QG}}{\partial t} + \overline{v_\psi' q_{QG}'} = \Delta M\left(\kappa \nabla^2 q_{QG}\right) \tag{9}$$

where $A_{QG} = \Delta M\left(q_{QG}\right)$. Following Edmon et al. (1980), the eddy vorticity flux can be separated into its horizontal and vertical wave fluxes, with some rearrangement, as

$$-\frac{\partial \overline{u'v'}}{\partial y} = -\frac{\partial A_{QG}}{\partial t} - f\frac{\partial}{\partial p}\left(\frac{\overline{v'\theta'}}{\partial\Theta/\partial p}\right) + \Delta M\left(\kappa \nabla^2 q_{QG}\right). \tag{10}$$

A second way is to define the tracer as absolute vorticity $f + \zeta$, so the absolute vorticity tendency budget becomes

$$\frac{\partial \zeta}{\partial t} + \vec{v}_\psi \cdot \nabla\left(f + \zeta\right) = -\nabla\left[\vec{v}_\chi \cdot \left(f + \zeta\right)\right] + \kappa \nabla^2 \zeta \tag{11}$$

where $\vec{v}_\chi$ is the divergent component of the flow, and $-\nabla\left[\vec{v}_\chi \cdot \left(f + \zeta\right)\right]$ is defined in Sardeshmukh and Hoskins (1988) as the Rossby wave source. Again, following (4), the eddy vorticity flux becomes

$$\overline{v_\psi' \zeta'} = -\frac{\partial A_\zeta}{\partial t} - \Delta M\left\{\nabla \cdot \left[\vec{v}_\chi\left(f + \zeta\right)\right]\right\} + \Delta M\left(\kappa \nabla^2 \zeta\right) \tag{12}$$

where $A_\zeta = \Delta M\left(\zeta + f\right)$. In a more general form for (10) and (12), the eddy vorticity flux may be written as a negative wave activity tendency, a wave source term S, and a wave dissipation term D,

$$\overline{v_\psi' \zeta'} = -\frac{\partial A}{\partial t} + S + D\,. \tag{13}$$

3.2 Conceptual Theory

With a closed model to describe eddy vorticity flux and hence annular mode variability, it is important to understand how each term in (13) contributes to shifts in the eddy-driven jet stream. Small-amplitude and finite-amplitude wave activity diagnostics share many analogies that provide a clear link to bridge the two theories. Fig. 1 depicts a schematic of the earth containing a zonally symmetric, midlatitude jet situated in a region of enhanced vorticity gradient; only one contour is demonstrated here. As a stirring mechanism interacts with the contour, it begins to deform and flux away from zonal symmetry, indicating a growth in wave activity. As the contour/waves flux meridionally away from the jet core, eddy voriticty fluxes in an opposite sense, indicating large amounts of momentum transfer. Depending on the preferential meridional propagation of waves, poleward or equatorward, the momentum transfer may shift or accelerate the zonal jet structure.

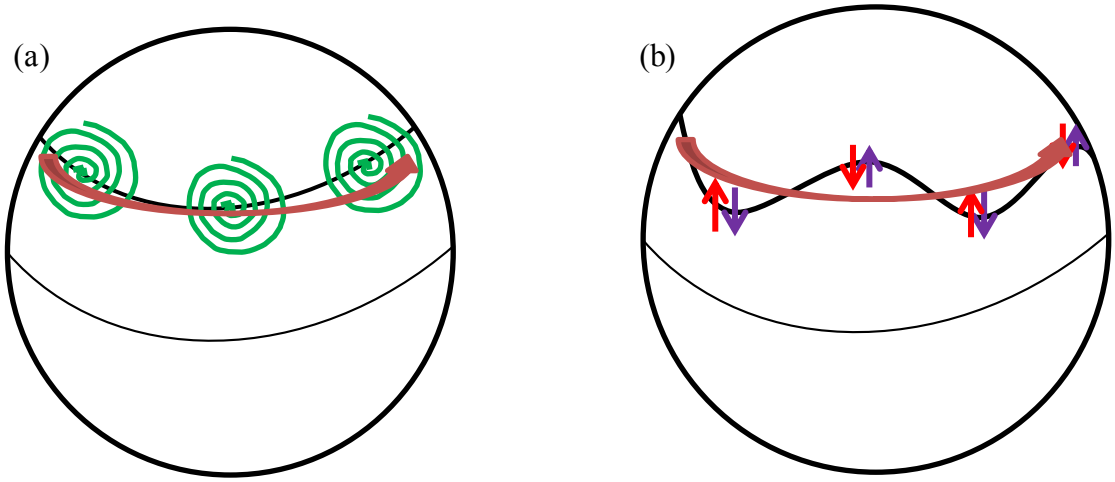

Figure 1: Schematic of small-amplitude wave activity for (a) time $t=t_o$ and (b) time $t=t_o+\Delta t$. Thin solid line is the equator; thick solid line is a vorticity contour; pink arrow is a midlatitude zonal jet; green arrows represent stirring or vorticity source; red arrows indicate eddy vorticity flux; purple arrows indicate horizontal wave tendency.

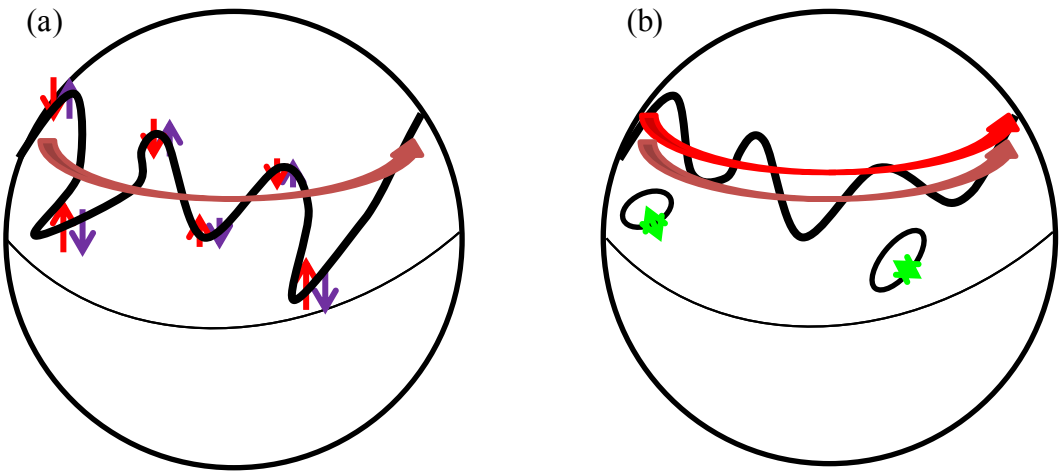

Figure 2: Same as Fig.1 except for finite-amplitude wave activity. Green arrows represent small scale dissipation. Red arrow indicates shifted zonal jet.

As these linear waves grow beyond a small-amplitude limit, the theory begins to break down. The use of the MLM in (5) has allowed the study of these finite-amplitude waves and their relation to the mean flow. Again, a zonally symmetric midlatitude jet in Fig. 2 is hit with stirring which again produces a growing wave away from zonal symmetry. In this case though, the wave can grow beyond the small-amplitude limit and may eventually produce meridional reversals in the vorticity gradient, indicating Rossby wave breaking. For a poleward shifting jet, there is a propensity for waves to flux preferentially equatorward. The majority of the momentum then is fluxing poleward producing a poleward shifting jet structure. And, as these equatorward waves grow and enter the large meridional shear of the mean flow, they break and leave large cut-off vortices, similar to Thorncroft et al. (1993), away from the shear of the zonal jet. These vortices can be slow to mix out with the background flow and may act to aid in the persistence of a zonal wind anomaly.

In the previous two schematics, stirring has ambiguously been added to initiate the wave fluxes necessary to simulate annular mode variability, but how does the redefinition of waves from QG PV to absolute vorticity change this physical stirring? From Edmon et al. (1980), QG PV wave stirring mechanism is proportional to the eddy heat flux v'T', and from Sardeshmukh and Hoskins (1988), absolute vorticity wave stirring is provided through the Rossby wave source term. This term is proportional to the horizontally divergent vorticity flux acting on a contour of vorticity. So QG PV waves stirring is supported from the lower-levels where eddy heat flux and baroclinicity maximize, whereas absolute vorticity wave stirring is supported at the upper-levels where horizontal wave fluxes maximize. Figure 3 demonstrates these aspects for a poleward shifting jet. For a poleward jet shift, a baroclinic zone typically develops on the poleward flank of a midlatitude jet. The eddy heat flux produces upward propagating QG PV stirring that reaches a vertical limit and propagates horizontally. It is the horizontal wave stirring that produces a signature for absolute vorticity waves. In this fashion, these wave stirring mechanisms together may act on a baroclinic jet to produce a poleward shifted jet. It will be shown that by defining waves with absolute vorticity, the source term is highly barotropic which suites it well for annular mode variability.

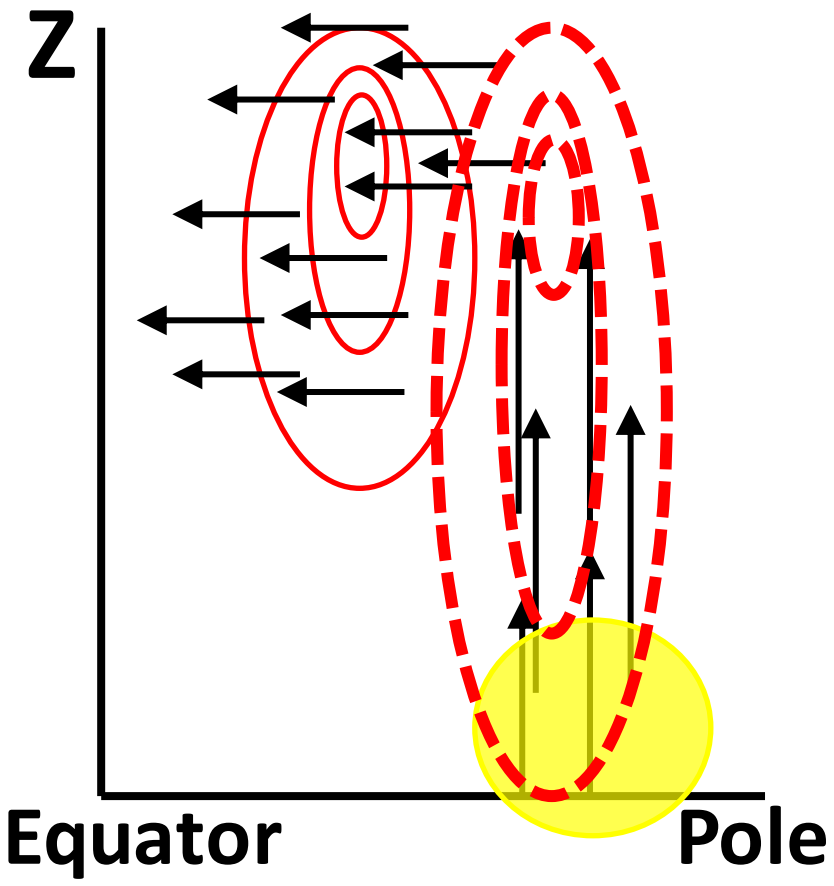

Figure 3: Schematic depicting a poleward shifting midlatitude zonal jet. Yellow circle represents a baroclinic zone; vertical arrows are QG PV stirring; horizontal arrows are absolute vorticity stirring; thin red lines are initial baroclinic jet; thick dashed lines are final shifted zonal jet.

CHAPTER 4

DATA AND METHOD

The baroclinic eddy lifecycle experiment will employ the atmosphere-only, GFDL spectral dynamical core model on 30 vertical sigma levels. There is no external heating or dissipation with only hyperdiffusion to damp out small scale enstrophy build up. More technical details about the model can be found in Solomon et al. (2012). The initial zonal-mean zonal wind is specified as in Hartmann and Zuercher (1998) as

$$u(\lambda,\phi,z) = u_o(\phi,z) + u_s(\phi) + u_m(\lambda,\phi,z) \tag{14}$$

where u_o is a baroclinic jet, u_s is a barotropic jet, and u_m is a velocity perturbation associated with the normal mode of zonal wave number, m. The baroclinic jet is specified as

$$u_o(\phi,z) = U_o \sin^3\left(\pi \sin^2\phi\right)\left[\frac{z}{z_T}\exp\left(-\frac{z^2/z_T^2 - 1}{2}\right)\right], \phi>0 \tag{15}$$

where U_o=45ms^{-1} and z_T =13km and the barotropic component of the initial wind as

$$u_s(\phi) = U_s\left\{\exp\left[-\left(\frac{\phi-\phi_e}{\Delta\phi}\right)^2\right] - \exp\left[-\left(\frac{\phi-\phi_p}{\Delta\phi}\right)^2\right]\right\}, \tag{16}$$

where ϕ_e=20°, ϕ_p=50°, and $\Delta\phi$=12.5°. One key to finding a transition between LC1 and LC2 is to systematically change U_s to explore the evolution of the effects of the normal mode perturbation. This study will use a zonal wavenumber of six and explore the same transition case as Solomon et al. (2012) which is U_s=9.5ms^{-1} for LC1 and U_s=10ms^{-1} for LC2. For the particular parameter regime this study will focus on, the zonal jet in LC1 exhibits a poleward shift and strengthening, while the LC2 zonal jet exhibits a slight equatorward shift and

strengthening (Solomon et al. 2012), consistent with observations of annular mode variability. This will be reestablished in Fig. 4 of the current study.

The GFDL dynamical core is an atmosphere-only, steady state model. Physical parameterizations are prescribed as in Held and Suarez (1994) with a Newtonian relaxation to a zonally symmetric equilibrium temperature profile and Rayleigh friction to damp the wind field in the planetary boundary layer. The model is run under equinox conditions at R30 horizontal resolution on 20 evenly space sigma levels. Integrations are performed for 6000 days. Other equilibrium temperature profiles are prescribed in Chapter 7 which alter the position of the climatological jet (Sun et al. 2013).

Momentum flux convergence budgets will be analyzed both barotropically, vertically integrated, and baroclinically, vertical cross sections. The following operator is applied to (13) and represents a mass weighted vertical integration

$$[\bullet(\phi,t)] = \frac{1}{p}\int_0^p \bullet(p,\phi,t)dp \tag{17}$$

simplifying (13) to

$$\left[\overline{v_\psi'\zeta'}\right] = -\frac{\partial[A]}{\partial t} + [S] + [D]. \tag{18}$$

To facilitate a momentum budget analysis in the dry model, principal component (PC) analysis will be performed using the vertical- and zonal-mean zonal wind, which is weighted by cos(ϕ) to account for converging meridians (Baldwin et al. 2009). The leading PC time series will be adapted as the zonal index to describe the leading mode of extratropical, atmospheric variability (Lorenz and Hartmann 2001). For barotropic cross sections, lag regressions using the zonal index will be used to examine how quantities contribute to the maintenance of an annular mode, zonal wind anomaly. For baroclinic cross sections, regressions are performed on non-

vertically averaged variables in (13). Regressions will also be performed onto the tendency of the zonal index to determine contributions exhibited by variables to the transition from one state of the jet to another, in this case a poleward shifting jet.

In addition to regressions, projections onto the leading empirical orthogonal function (EOF) latitudinal structure are used to determine the various contributions to annular mode variability. Adopting similar notation to Simpson et al. (2013), the projection is defined for a vertically and zonally averaged field $[\bar{x}](t,\phi)$ as

$$[\bar{x}]_{AM}(t) = \frac{[\bar{x}](t,\phi)\mathbf{We}}{\sqrt{\mathbf{e}^T\mathbf{We}}} \tag{19}$$

where **W** is a diagonal weighting matrix loaded with cos(ϕ) (Baldwin et al. 2009), **e** is the EOF structure associated with the zonal index, and $[\bar{x}](t)$ is the portion of $[\bar{x}](t,\phi)$ that projects onto the latitudinal structure of the annular mode. Since this model is hemispherically symmetric, the distinction between the northern annular mode (NAM) and southern annular mode (SAM) is ambiguous, hence the use of AM. After applying (19), (18) becomes

$$[\overline{v_\psi'\zeta'}]_{AM} = -\frac{\partial[A]_{AM}}{\partial t} + [S]_{AM} + [D]_{AM} \tag{20}$$

.

This provides time series of momentum flux convergence budget terms that describes the temporal eddy variability associated with the annular mode structure. Covariance structures between these eddy time series and the zonal index will be used to determine the temporal contributions to variability. (19) can then be applied directly (13) to provide eddy-mean flow feedback cross sections. Questions about zonal index variability can be analyzed using the covariance structures and vertical cross sections, particularly, what projects onto the positive feedback associated with the persistence of the zonal wind anomaly?

CHAPTER 5

RESULTS

5.1 Baroclinic Lifecycle Experiment

A preliminary investigation of the baroclinic lifecycles begins with the zonal-mean zonal wind and Rossby wave breaking. The first column of Fig. 4 plots the zonal-mean zonal wind evolution for both lifecycles as well as wave breaking frequency on the 290hPa surface. The second column of Fig. 4 illustrates the horizontal structure of both cyclonic wave breaking (CWB) and anticyclonic wave breaking (AWB) on day 14 for the lifecycles. Initially both lifecycles, LC1 in row 1 and LC2 in row 2, are characterized by midlatitude jets situated just poleward of 40°N with the slightest hint that LC2 is initialized with more cyclonic shear from a single negative contour near 80°N. It is around day 14 that the zonal jet patterns in each lifecycle diverge with the jet in LC1 accelerating poleward of its initial location and LC2 accelerating at its initial latitudinal location. Evident in column 2, the enhanced meridional vorticity gradient pattern on day 14 suggests an undulating jet structure with large-scale reversals in the vorticity gradient indicating CWB on the poleward flank of the jet and AWB (red circles) on the equatorward flank of the jet. These spatially oriented features are apparent in column 1, where both flows develop CWB around day 8 and AWB around day 12 on respective flanks of the jet. After this day, LC1 develops more AWB, while LC2 develops more CWB. In the regions of enhanced wave breaking where maximal mixing occurs, easterly flow develops flanking an accelerating zonal jet in both lifecycles. Concurrent with the wave breaking and mixing is a meridional shift in the LC1 zonal jet to near 50°N, whereas the zonal jet in LC2 remains latitudinally confined. In summary, the growth and rearrangement of waves following

an initial perturbation provides the necessary momentum fluxes to shift and/or accelerate a zonal jet. Following the initial shift, prolonged wave propagation and wave breaking continue to provide the momentum flux to persist the jet at its new location. These features are evident in many other studies of jet stream variability.

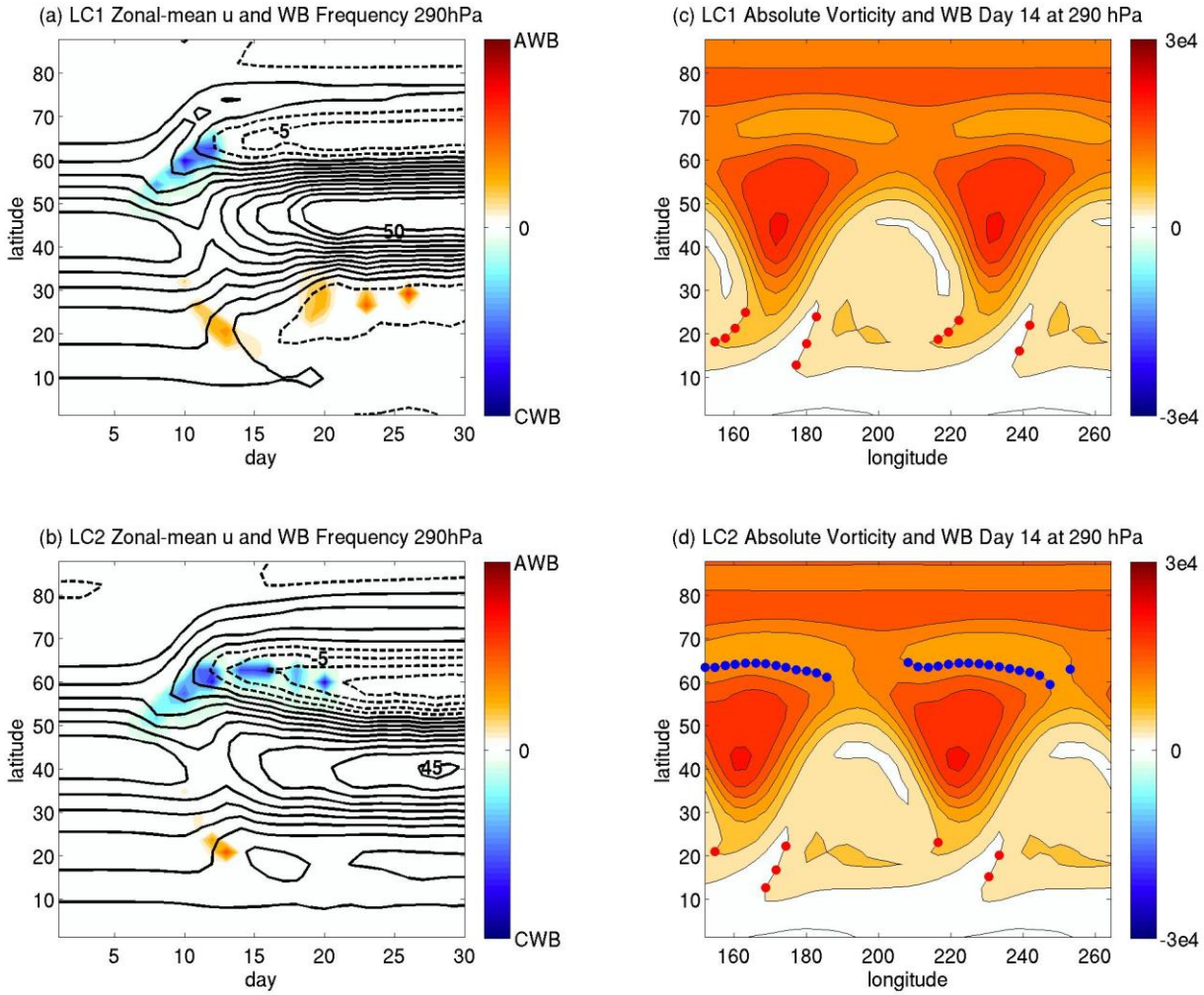

Figure 4: Zonal-mean zonal wind (contours) and wave breaking frequency (shades) at 290hPa for (a) LC1 and (b) LC2 and absolute vorticity (shades with contours) and wave breaking (red dots for AWB and blue dots for CWB) at 290hPa on day 14 for (c) LC1 and (d) LC2.

An analysis of (18) for absolute vorticity and QG PV is performed in Fig. 5 to confirm the validity of the budget as well as to quantify the contributions to barotropic, eddy vorticity flux. Plotted for both cases is LC1 minus LC2 which represents a poleward shifting and

accelerating jet. The zonal jets diverge, as mentioned, around day 14 and represent a strongly barotropic, meridionally shifted jet. Note that eddy momentum flux convergence describes well the zonal-mean flow acceleration, and both quantities are the same for QG PV and absolute vorticity. The contributions from the RHS of (18) will not be the same though. Figure 5e confirms the eddy-driven nature of the zonal wind shift. Wave tendency indicates equatorward wave fluxes and shows a strong dipole structure that describes the majority of the zonal-mean flow dipole. The source terms do not contribute to the dipolar structure of the zonal-mean flow but do provide the waves necessary to differentiate LC1 from LC2. Relatively enhanced dissipation in LC1 around day 20 reflects the presence of AWB and small scale dissipation in the previous figure. So for a poleward shifted and maintained jet in this eddy lifecycle experiment, it is the barotropic wave tendency that contributes most to the momentum flux convergence with dissipation from wave breaking providing support in the deceleration region.

First noted by Simmons and Hoskins (1980) as their anomalous case, by increasing the barotropic shear on a baroclinic jet, eddy kinetic energy can exhibit similar, large baroclinic growth but relatively slow barotropic decay when compared to their basic state. This is perceived with a glance at Fig. 5 where the growth characteristics of the lifecycles are strikingly similar; look for regions with no contours prior to day 10. It is then the decay of these growing lifecycles that provide the momentum for a jet shift. To better understand the momentum fluxes, vertical cross sections of day 18 minus day 13 will be used. This time period represents the majority of the eddy momentum flux convergence and wave tendency dipole structures.

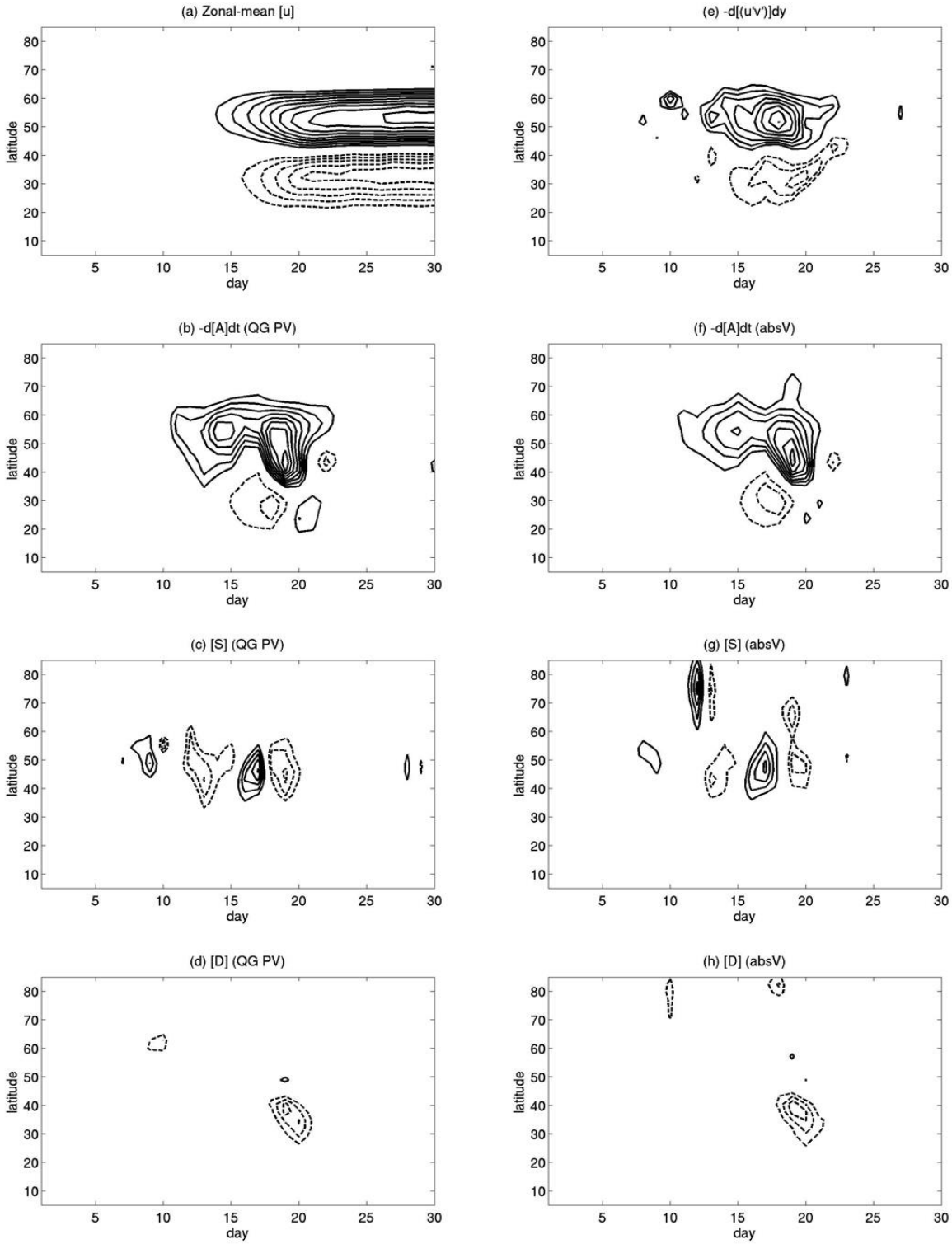

Figure 5: (a) Zonal-mean zonal wind in ms^{-1}; (e) Eddy momentum flux convergence in $ms^{-1}day^{-1}$; (b) –d[A]dt, (c) [S], and (d) [D] for QG PV waves; (f) –d[A]dt, (g) [S], and (h) [D] for absolute vorticity waves. All plots are LC1 minus LC2.

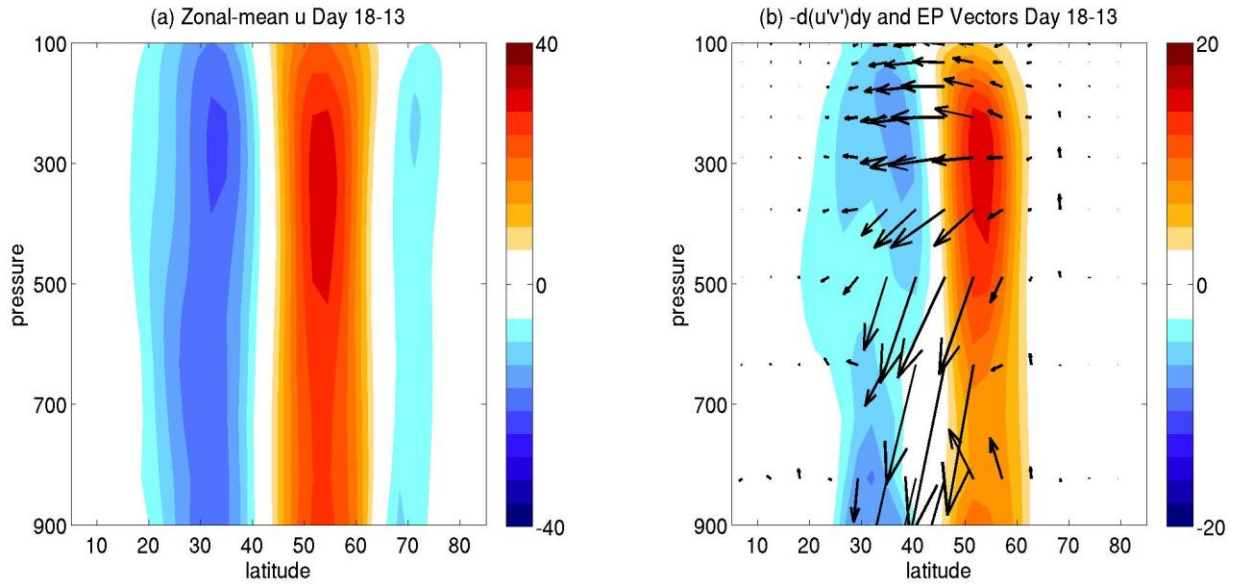

Figure 6: Day 18 minus day 13 for (a) zonal-mean zonal wind in ms^{-1} and (b) eddy momentum flux convergence and EP- vectors (arrows) in $ms^{-1}day^{-1}$ for LC1 minus LC2.

Figure 6 plots the difference between day 18 and day 13 for the zonal-mean zonal wind, eddy momentum flux convergence, and EP vectors (Edmon et al. 1980) for LC1 minus LC2, which are the same for QG PV and absolute vorticity. The zonal-mean zonal wind is characterized as an eddy-driven, barotropic, and poleward shifted zonal-mean wind. The EP vectors provide insight into the strong barotropic structure of the eddy momentum fluxes, especially above 500hPa. The upper level momentum convergence is provided by the equatorward fluxing waves whereas the lower level convergence is provided by both baroclinic growth in the jet region and strong baroclinic decay into the subtropics. The absolute vorticity wave source describes the horizontal component of the diverging waves, and QG PV wave source describes the vertical component of the diverging waves. Either way, there is a strong horizontal component to the wave fluxes representing a barotropic jet. The next figure will focus above this 500hPa level since the balance associated with (18) is well satisfied here.

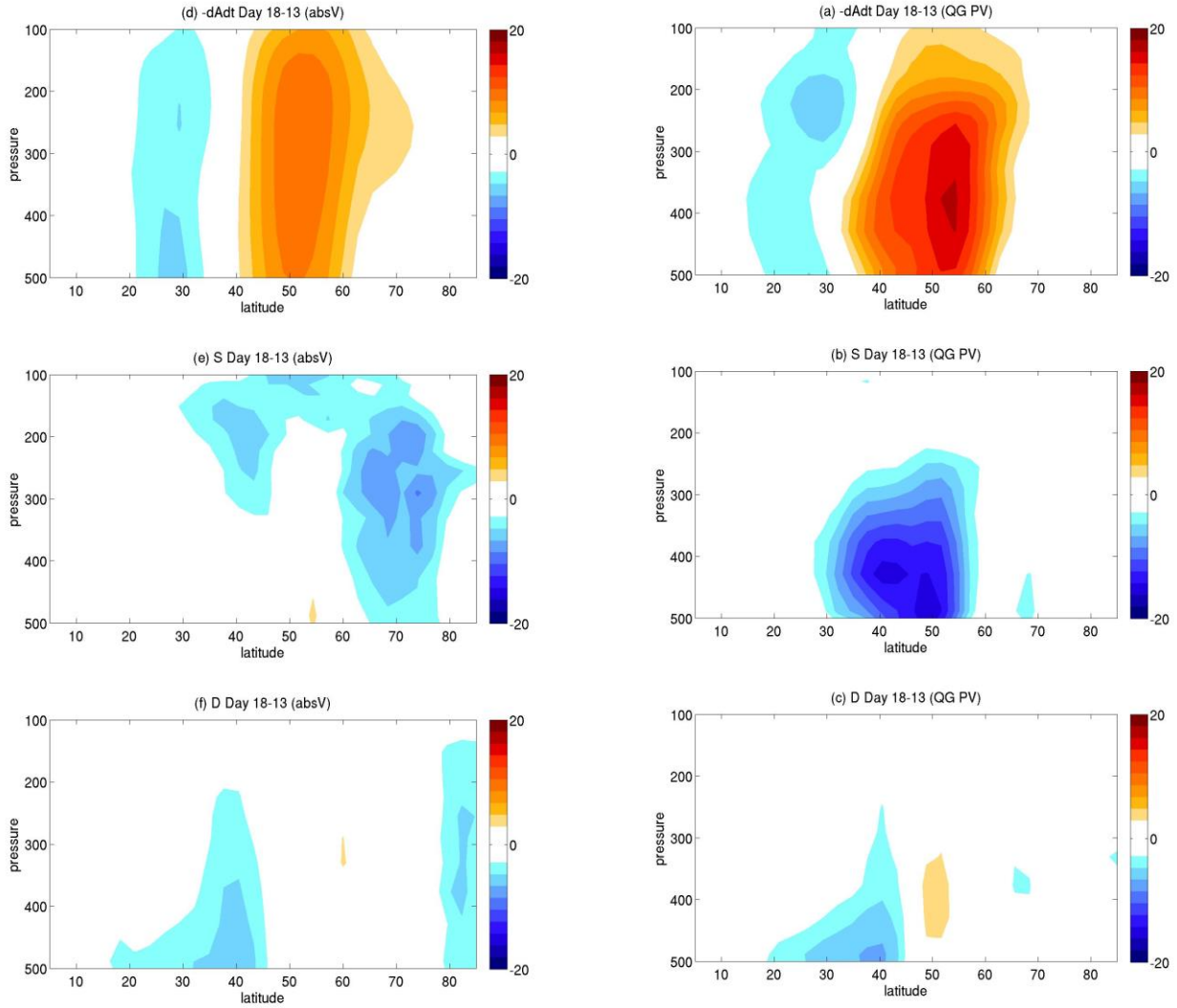

Figure 7: Same as Fig. 6 but for (a) –dAdt, (b) S, and (c) D for QG PV waves and (d) –dAdt, (e) S, and (f) D for absolute vorticity waves, all in $ms^{-1}day^{-1}$. Note the vertical axis is restricted to 100 to 500hPa in contrast to Fig. 6.

Figure 7 plots (13) for day 18 minus 13 above the 500hPa level for LC1 minus LC2. In agreement with Fig. 4, the wave tendency provides much of the dipole structure associated with the zonal wind shift with dissipation providing some support in the deceleration region. A large depletion of waves near 50°N essentially zonalizes the vorticity contours and allows for zonal flow acceleration. The source terms are in agreement with the EP vectors in Fig. 6. Two zones of diverging waves, downward for QG PV waves and equatorward for absolute vorticity waves,

provide the evacuation of waves necessary to zonalize and accelerate the flow. On the equatorward flank of these diverging waves, dissipation is enhanced where suspected AWB occurs. A high latitude maximum in the absolute vorticity source term is unclear at this point. It is the signature presented by fluxing waves that provides the wave tendency with a dipole structure similar to the eddy momentum flux convergence.

With the balances well satisfied for (13) and (18), focus will now shift to a steady state model to determine the contributions that eddy-mean flow or wave-mean flow feedbacks have on the unusual persistence or self-maintenance (Robinson 2006) of zonal-mean flow anomalies.

5.2 Dry Model

5.2.1 Zonal Index Persistence

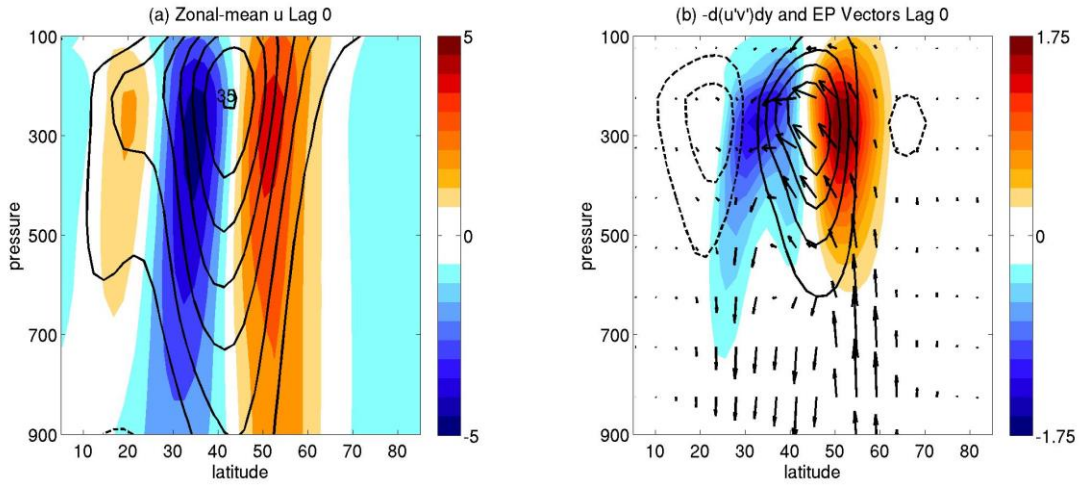

Figure 8: Climatologies (contours) and lag 0 regressions onto the zonal index (shades) for (a) zonal-mean zonal wind in ms^{-1} and (b) eddy momentum flux convergence with EP-vectors (arrows) in $ms^{-1}day^{-1}$.

This section begins with an analysis in Fig. 8 of the zonal-mean zonal wind, eddy momentum flux convergence, and EP vector climatologies as well as the lag 0 regressions onto the zonal index, which will be called eddy variability. Consistent with observations of extratropical variability, the climatological jet is situated around 200hPa and 40°N consisting of a baroclinic and barotropic structure. Hints of a highly baroclinic subtropical jet are also evident in the subtropics. The momentum flux convergence dipole confirms the eddy-driven nature of the midlatitude jet. The eddy variability consists of a poleward, barotropic shift of the midlatitude jet which is consistent with momentum flux convergence. Similar to the lifecycle experiments, this anomalous zonal jet coincides with a baroclinic source of waves at the same latitude of the eddy jet. These waves flux into and equatorward of the climatological jet before diverging to a wave sink near the surface in the subtropics. In general, this run of the dry model

is consistent with other extratropical variability studies including experiments, models, and observations. An analysis of the climatologies and eddy variability's of the RHS of (13) will be deferred until the discussion of positive feedbacks below.

A look at the barotropic temporal evolution of (18) using lag regressions onto the zonal index will provide insight into the mechanisms associated with the persistence of a meridionally shifted zonal jet. Negative lags describe eddies leading the zonal index, and the opposite is true for positive lags. The barotropic zonal jet in Fig. 9a is again shown to be eddy-driven and consists of a meridional dipole extending beyond +/- lag 30. An abrupt increase in the convergence of momentum occurs 2 days prior to the zonal index but also extends beyond +/- 30 days, similar to linear models of positive eddy-mean flow feedback (Lorenz and Hartmann 2001; Simpson et al. 2013). A striking feature for zonal flow persistence is the lack of persistence associated with wave tendency. Whereas all of the quantities in (18) extend for this entire period, wave tendency is a short-lived event. In reference to these linear models, the wave tendency contributes to the burst of eddies that shift the zonal jet, whereas the source and dissipation terms consist of eddy memory that prolongs the zonal jet shift. This is confirmed with the plots of source and dissipation that extend through the +/- lag 30 domain, similar to the zonal flow and eddy momentum convergence. The source and dissipation of waves both contribute to support the zonal flow anomaly at its poleward location.

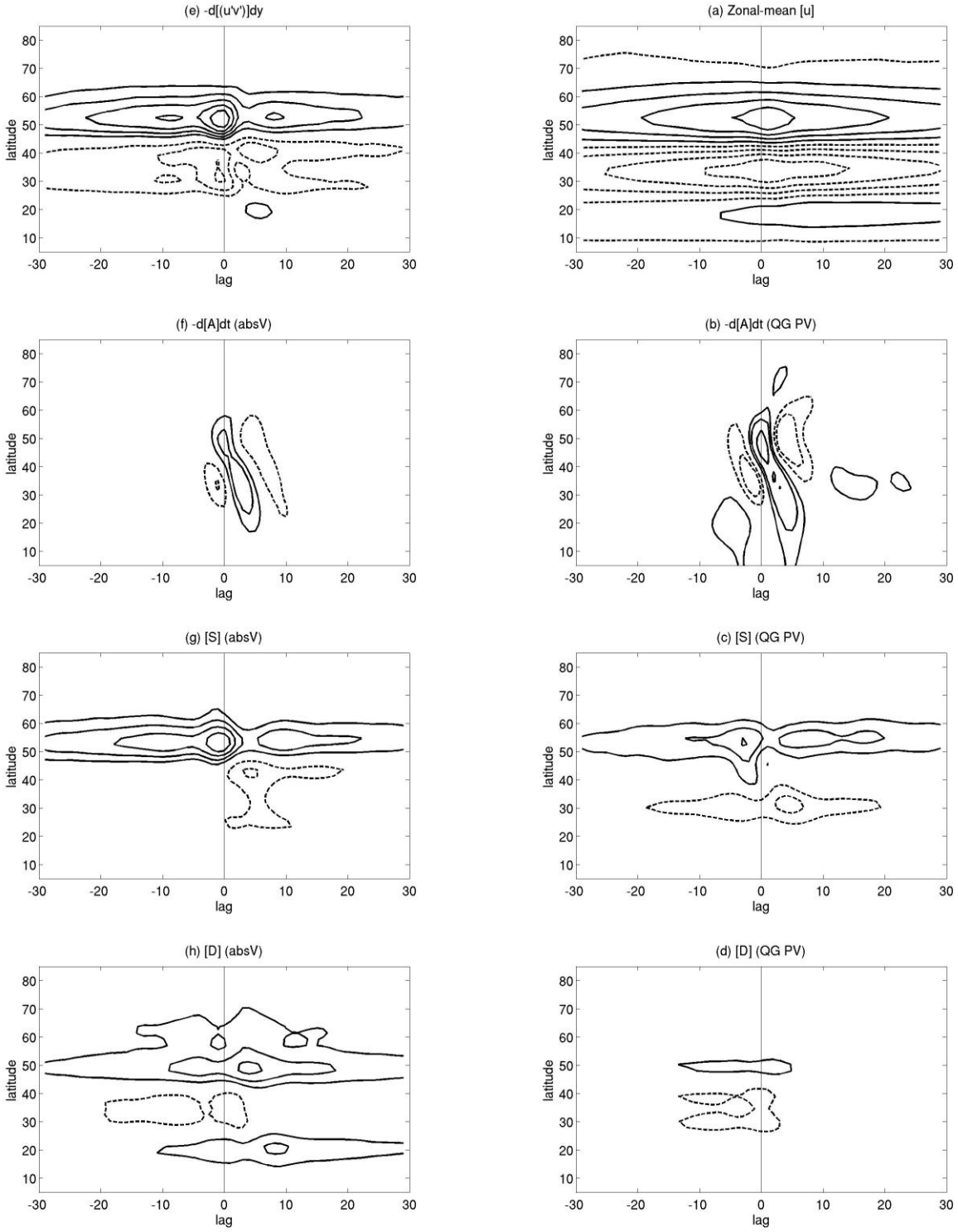

Figure 9: Lag regressions onto the zonal index for (a) zonal-mean zonal wind in ms^{-1}, (b) eddy momentum flux convergence in $ms^{-1}day^{-1}$, (c) –d[A]dt, (d) [S], and (e) [D] for QG PV waves, and (f) –d[A]dt, (g) [S], and (h) [D] for absolute vorticity waves.

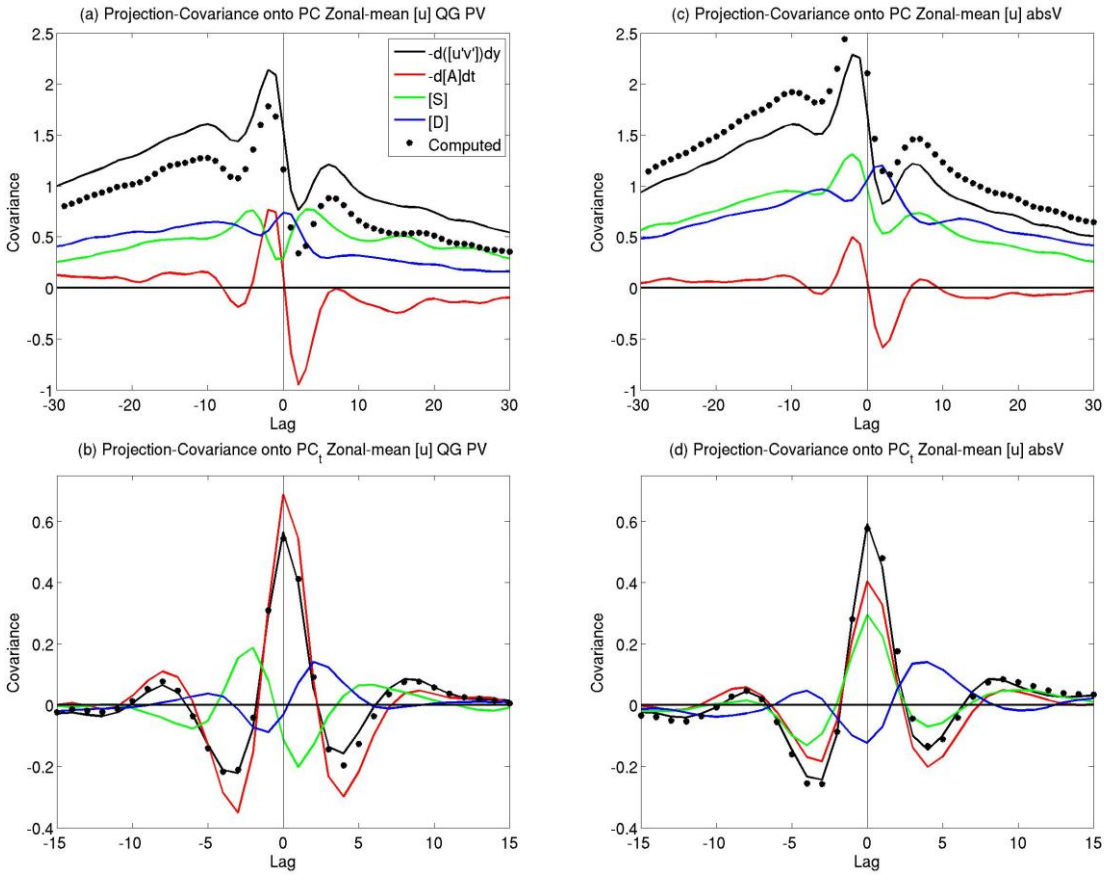

Figure 10: Cross-covariance structures of (18) for (a) the zonal index and (b) tendency of the zonal index for QG PV waves and (c) the zonal index and (d) tendency of the zonal index for absolute vorticity waves. Note the different temporal scales used for the zonal index and its tendency. See figure for color scheme.

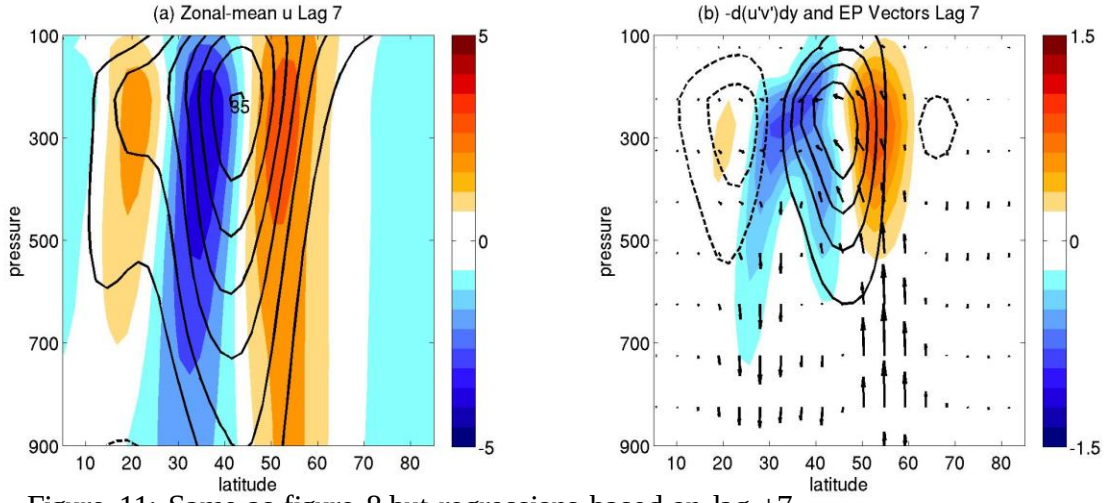

Figure 11: Same as figure 8 but regressions based on lag +7.

The first row of Fig. 10 plots the covariance structures of eddy time series in (20) with the zonal index to confirm the previous temporal structure. Again, the eddy forcings lead the zonal index for negative lags, and vice versa. In agreement with Fig. 9, a burst of eddy activity associated with wave tendency leads the zonal index by a couple days. The wave tendency quickly decays and damps the zonal index before settling into a small damping for the remainder of the period. The momentum flux convergence has a similar high frequency response acting to accelerate the flow but also exhibits another peak near day 7. This is the positive feedback region that is independent of the initial burst of eddies and constitutes a feedback associated with the zonal index anomaly (Lorenz and Hartmann 2001). Both the source and dissipation terms provide positive support to this feedback mechanism. The temporal aspects are quite similar between QG PV and absolute vorticity waves except the source term. Baroclinic QG PV waves are first generated in the vertical before turning equatorward. Once turning equatorward a response will trigger for a source of absolute vorticity waves, thus the delay. Physically, baroclinic QG PV waves flux into the jet acting to decelerate it, whereas barotropic absolute vorticity waves flux outward from the jet acting to accelerate it. This is well represented in Fig. 10.

Figure 12 plots the zonal-mean zonal wind, eddy momentum convergence, and EP vectors for lag +7; so the zonal index leads the eddies. The reason for deferring the climatologies of (13) can be understood by comparing Fig. 11 with Fig. 8. The feedback plots for these three variables look nearly identical to lag 0 regressions just slightly weaker in magnitude. This reinforces the zonal wind anomaly and allows for its persistence. The same can be said about feedback plot in Fig. 12 when comparing it to the lag 0 regressions; note wave tendency was too small to show. The feedback of the mean-flow onto the eddies appears quite

similar to the effect of the eddies on the mean flow. The climatological source terms also confirm the covariance structures in Fig. 10. The climatological baroclinic and barotropic waves for QG PV and absolute vorticity, respectively, support the zonal flow climatology with climatological momentum flux convergence. The barotropic waves diverge across the climatological jet, whereas the baroclinic waves converge on the poleward flank of the jet. A broad peak in absolute vorticity dissipation occurs on the poleward flank of the jet and extends into the subtropics indicating a wide range of small scale mixing as the jet wobbles about its climatological position. Enhanced dissipation of QG PV waves may be an artifact of QG breakdown in the tropics. The eddy variability associated with the persistence is of greatest interest. The baroclinic waves show enhanced convergence at the latitude of the jet which tilts equatorward with height. The waves then strongly diverge toward the surface in agreement with Fig. 11. On the other hand, the source of absolute vorticity waves is a highly barotropic, poleward shift of the diverging waves. Both the shift in baroclinicity and the barotropically developing waves coincide with the meridional extent of the zonal wind anomaly. The dissipation of barotropic waves minimizes at the jet axis and again in the subtropics where signature of an eddy driven jet also exists, see Fig. 11. Baroclinic waves show a maximum in the subtropics just equatorward of the upper level converging waves. Together, the dissipation of barotropic and baroclinic waves represents a picture consistent with equatorward wave propagation, breaking, and mixing. It is interesting that enhanced dissipation with respect to the climatology only occurs in baroclinic waves while reduced dissipation occurs only with barotropic waves. So consistent with the covariance structures in Fig. 10, the source and dissipation of waves both act to support the zonal flow anomaly which is independent of the zonal flow anomaly itself.

In summary for the zonal index persistence, a short-lived burst of waves can be considered the stochastic forcing onto the zonal index, and the source and dissipation term can be considered the linearly dependent feedback mechanisms (e.g. Lorenz and Hartmann 2001; Simpson et al. 2013). Without having to perform time filters, it appears the waves act as a short term, synoptic forcing, while the source and dissipation act as a long-term, feedback forcing on the zonal index.

5.2.2 Zonal Index Transition

By using the time-derivative of the zonal index, insight can be gained into how the terms in the eddy momentum budgets contribute to the shift of the zonal index. Figure 13 plots (18) over +/- 15 days which is half the domain associated with the persistence of the zonal index. Again, the jet described by the tendency of the PC is driven by eddy momentum flux convergence/divergence dipoles. In contrast to the PC plots, the temporal structure of (18) is short-lived with no response outward of +/- 10 days. For both formalisms, it is contributions from the source term and wave tendency that supply the momentum fluxes necessary to shift a zonal jet. Since the baroclinic waves are vertical, the QG PV source term leads the zonal index but is in phase with respect to absolute vorticity waves. The quick burst of eddies associated with the zonal wind shift can be attributed mostly to the wave tendency for QG PV and wave source and tendency for absolute vorticity. This is confirmed in the second row of Fig. 10 which is the covariance structures associated with the tendency of the zonal index. The QG PV source leads the zonal index and the wave tendency contribute nearly completely to the momentum flux convergence. The absolute vorticity source develops along with the wave tendency and momentum convergence.

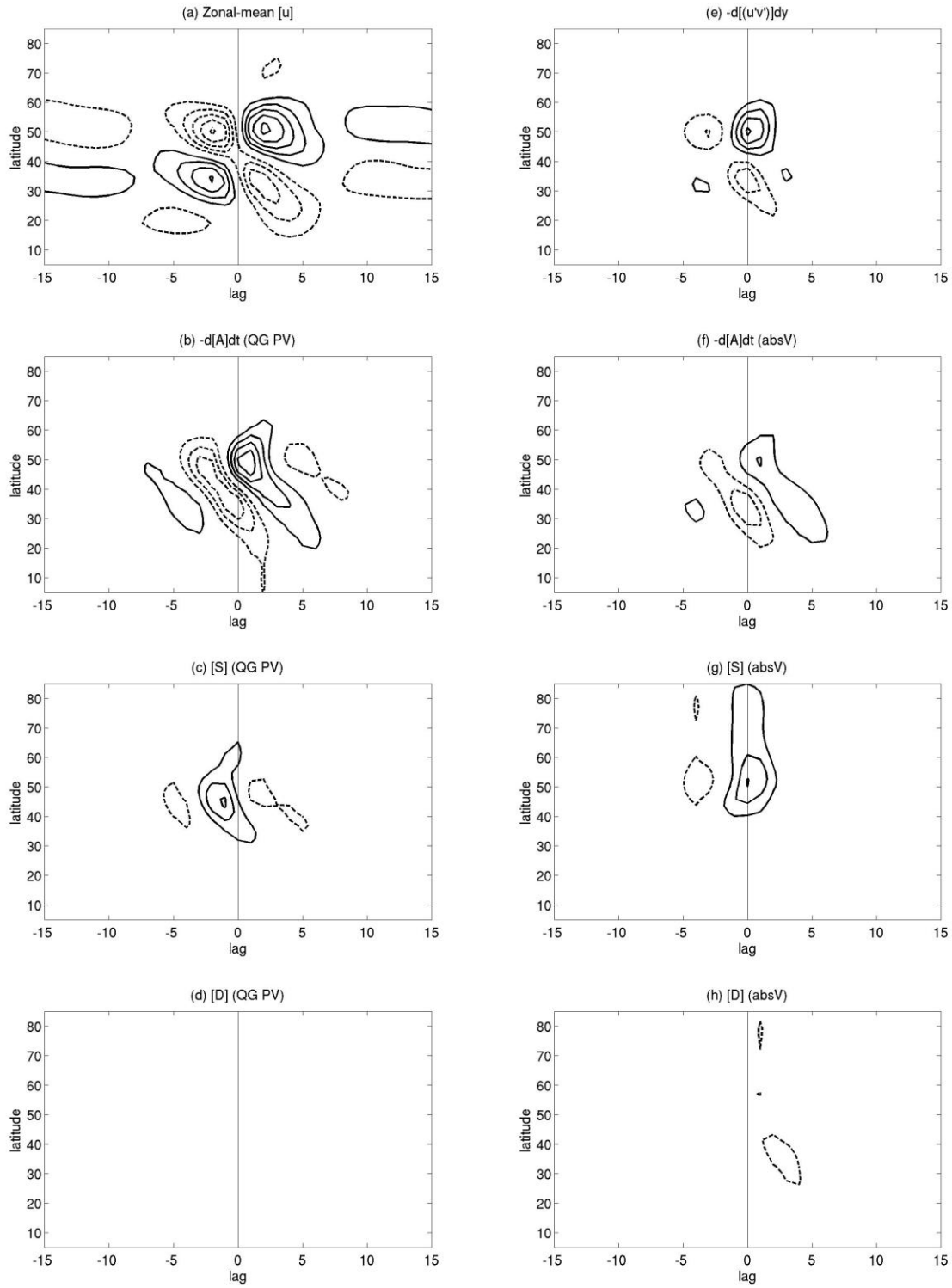

Figure 12: Same as figure 9 but regressions based on zonal index tendency. The horizontal axis extends to +/- 15 days in contrast to figure 9.

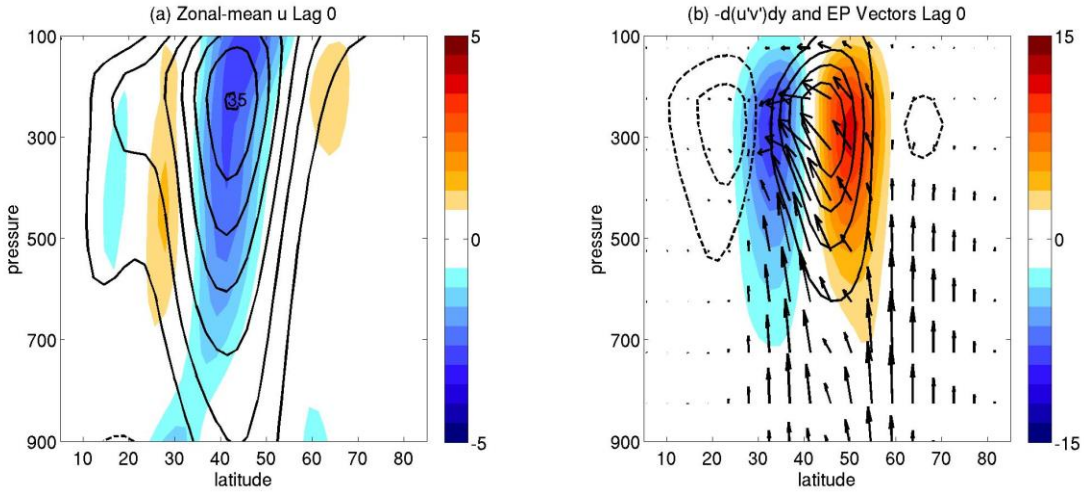

Figure 13: Same as figure 8 but regressions based on zonal index tendency.

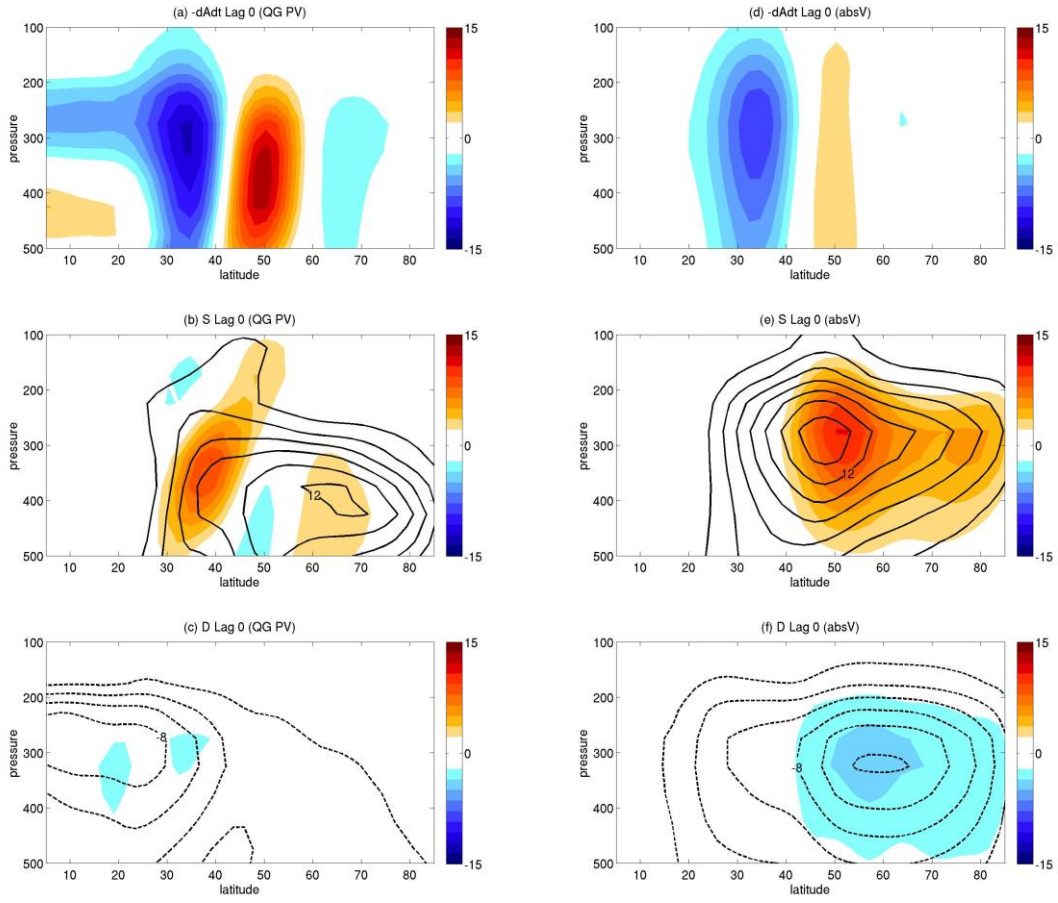

Figure 14: Climatologies (contours) and lag 0 regressions onto the tendency of the zonal index (shades) for (a) –dAdt, (b) S, and (c) D for QG PV waves and (d) –dAdt, (e) S, and (f) D for absolute vorticity waves all in $ms^{-1}day^{-1}$.

The vertical structure of the zonal-mean zonal wind, momentum flux convergence, and EP vectors are plotted in Fig. 13 for lag 0, the day of zonal index transition. The baroclinic source of waves from the surface first acts to decelerate the climatological jet. The barotropic waves then act horizontally to convergence momentum into a poleward shifting jet. By lag +1, not shown, the jet has strongly accelerated at its eddy latitude. The difference between the positive feedback plot and the jet shift plot is the wave fluxes associated with the EP vectors. There is no longer a subtropical baroclinic sink of waves but now a baroclinic source acting to converge even more waves into the climatological jet. This helps to provide the large amount of momentum flux necessary to shift the jet. As expected, Fig. 15 confirms that the wave tendency and source term contribute the majority of the momentum to shift the jet poleward. A large decrease in waves at the eddy jet core zonalizes the vorticity contours and thus indicates jet acceleration. A large increase in waves on the equatorward flank of the jet indicates momentum fluxing poleward into the eddy jet. The vertically propagating subtropical waves are shown to converge in the subtropics, while the barotropic waves horizontally fluxes away from the jet core. A high latitude source of absolute vorticity waves may explain the enhanced dissipation in Fig. 15f. So the source and tendency of waves provide the signature dipole structure associated with the shift the zonal jet.

CHAPTER 6

CONCLUSION

The annular mode spatial and temporal structures were analyzed using two eddy momentum convergence closure budgets for an eddy lifecycle experiment and a run from a GFDL steady state model. The shift and subsequent persistence of a zonal jet were the primary focuses to determine how QG PV and absolute vorticity waves affected the mean flow differently. While many similarities existed between wave tendency and dissipation fields, wave source and sink regions exhibited differences due to the orientation of flux.

The lifecycle experiment showcased growing baroclinic waves that turned either equatorward or poleward as barotropic waves near the jet core. It was shown that the wave tendency provided the majority of the signature for a zonal wind shift. Since wave activity is calculated on isobaric surfaces, positive wave tendency denotes regions where waves are horizontally propagating into. As barotropic waves flux away from the jet core and flux momentum into the jet core, the waves enter regions of large meridional shear and tend to break. These breaking waves leave cut-off vortices, spatially larger for CWB in LC2, lasting from day 10 through the day 30 of the calculation. In summary, an initial deceleration of the flow ensues from baroclinic wave convergence, followed by barotropic wave divergence, accelerating and shifting the flow. The slowly dissipating vortices leftover from wave propagation divert the mean flow and remain long-lived away from the shear of the jet, providing persistence. With no external maintenance of baroclinicity such as Newtonian temperature relaxation as in the steady state model, this eddy-jet can be designated as self-maintaining (Robinson 2006).

Use of a GFDL steady state model allowed a more quantitative approach to analyze not only the spatial structure associated with eddy variability but its temporal aspects. Previous work has decomposed the eddy variability into an independent burst of wave activity followed by a linearly dependent decay of the zonal index (Lorenz and Hartmann 2001). This allows

separation of annular mode variability into a burst of waves that sets the latitude of the eddy variability followed by a decay that sets the timescale of persistence. Through the use of a Lagrangian-mean perspective, these temporal structures can be showcased in two eddy momentum convergence budgets. Without spectral filtering into high- and low-frequency components, it appears the horizontal wave tendency provides the short-lived shift and acceleration of the jet, while the sources and dissipation of waves provide the long-lived persistence of the jet. This is in qualitative agreement with the lifecycle experiment which only describe a single eddy event.

An initial goal of this study was to perform an analysis of QG PV versus absolute vorticity wave dynamics where large discrepancies between how the different definitions of vorticity affected wave propagation were hypothesized (Riviere 2009). For the waves in these two idealized models, there were few major discrepancies. As mentioned throughout the text, the dynamics associated with absolute vorticity waves tend to be much more barotropic which is most likely a consequence of the source term defined in the horizontal. Absolute vorticity waves also eliminated issues with using QG PV dynamics in the tropical regions. The redefinition of a wave source term, of course, affects the signature of both the waves and their source region. QG PV wave source propagates vertically from the surface at the latitude or just poleward of the jet, while absolute vorticity source is horizontal and just poleward of the upper-level jet core. To complement and extend this study, an analysis of climatological jets located at different latitudes will be performed. The latitude of the climatological jet has been shown to affect wave propagation and therefore eddy feedbacks (Barnes and Hartmann 2011). A preliminary investigation has shown a dependency of zonal index persistence on jet latitude and speed, so further work will be performed in this area. Through the use of QG PV and absolute vorticity wave definitions, insight into the effect of vorticity definition on wave propagation can be gained for jets located at different latitudes with different magnitudes.

CHAPTER 7

FUTURE WORK

Recent attention into annular mode variability has focused on the influence of the latitude of the climatological jet on eddy-mean flow interaction, more specifically, the persistence associated with the annular modes (e.g. Barnes et al. 2010; Barnes and Hartmann 2010; Garfinkel et al. 2012; Simpson et al. 2013ab; Sun et al. 2013). By using the same steady state, GFDL model introduced above, insights into the dependence of eddy-mean flow feedback on climatological jet position hoped to be gleamed. As the climatological jet shifts poleward, the leading mode of variability transitions from a north-south shift to a pulse in magnitude. One mechanism to explain this is the reduction of wave breaking on the poleward flank of a poleward jet due to increased eddy-length scales (Barnes and Hartmann 2010 and 2011). Also, the influence from an eddy-mean flow feedback was shown to produce the poleward shifted response of the annular modes to global warming like temperature anomalies in an idealized model (Sun et al. 2013). Although Simpson et al. (2013) showed that improving the climatological jet position from an equatorward biased state does not fully alleviate the excess persistence of the annular mode. A suite of tropical temperature gradient experiments used in Sun et al. (2013) will be analyzed to motivate the use of the MLM to better understand the timescales of persistence associated with climatological jet position.

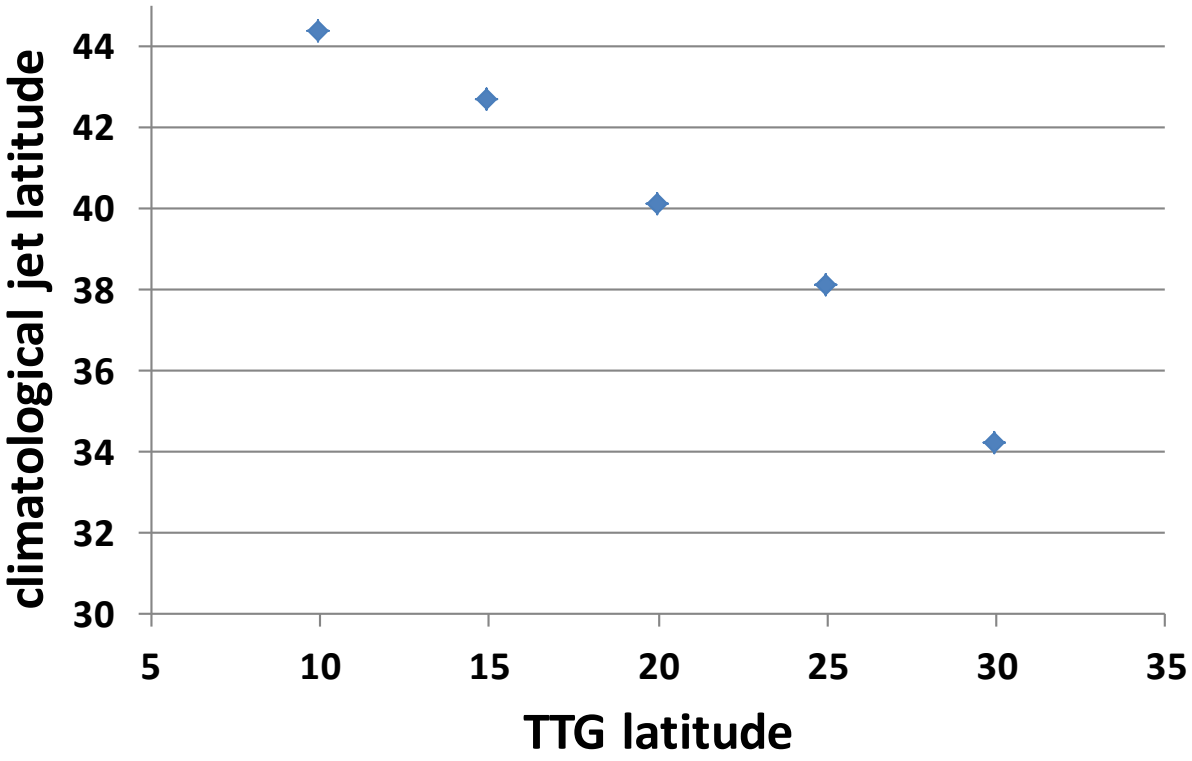

Figure 15: Climatological (time-mean) jet latitude as a function of tropical temperature gradient (TTG) latitude.

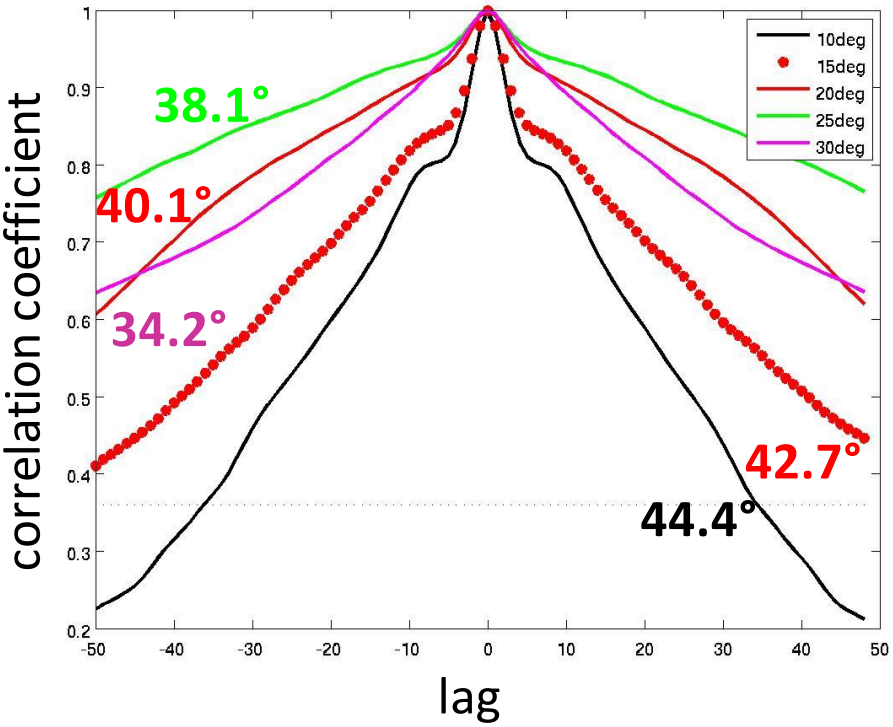

Figure 16: Autocorrelation function of the zonal index for different arrangements of tropical temperature gradient. Labels are provided within the figure. Plotted next to each contour is the climatological jet latitude from the previous figure.

A few of the details of the experiments are given here with extended detail in Sun et al. (2013). An enhancement of the tropical temperature gradient (TTG) is used to mimic the effects of global warming like scenarios. A parameter to alter the latitude of the TTG is used which indirectly affects the latitude of the climatological midlatitude, eddy-driven jet. Fig. 15 plots the time-mean jet's latitude as a function of TTG latitude. The latitude of the time-mean, climatological jet is calculated at the 290hPa level where maximum amplitude is achieved. As the latitude of the TTG increases, the latitude of the climatological jet decreases. With this knowledge, aspects of eddy-mean flow interaction can be analyzed with varying jet latitudes. To motivate future research, lag autocorrelations were performed on the leading principal component time series, the zonal index from above. Figure 16 agrees with aspects presented in other papers of the dependence of jet latitude on persistence of the zonal index (e.g. Barnes and Hartmann 2010; Barnes et al. 2010; Garfinkel et al. 2012; Simpson et al. 2013). The dependence of jet latitude on persistence does not appear to be linear. Initially, when increasing from 34.2° to 38.1°, the zonal index becomes more persistence; the autocorrelation function decays slower. Then in agreement with previous studies, as the jet latitude increases, the persistence decreases from an e-folding day of well over 50 days to under 40 days. E-folding is the day at which the autocorrelation function reduces to below 1/e. Figure 17 shows two groupings similar to the previous figure. With the jets located in at a lower latitude, the eddy-mean flow feedback is greatly enhanced leading to overly persistence jets. The eddy forcing for the jets located at 42.7° and 44.4° decays much more rapidly than the low latitude jets. The feedback is still there but decays quicker. Future works hopes to use diagnostics presented in this study to analyze why annular mode persistence depends on the latitude of the climatological jet.

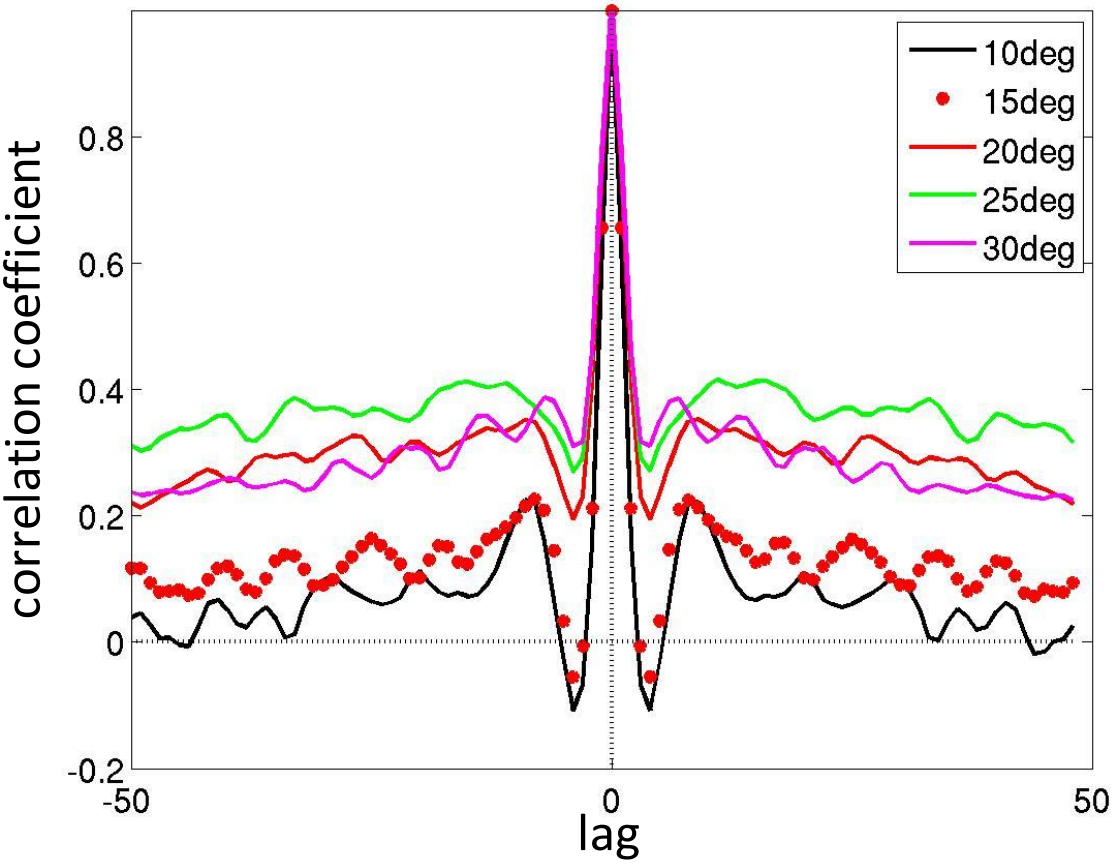

Figure 17: Same as Fig. 16 but for eddy vorticity flux.

REFERENCES

Arakelian, A. and F. Codron, 2012: Southern Hemisphere Jet Variability in the IPSL GCM at Varying Resolutions. *J.Atmos.Sci.*, **69**, 3788–3799.

Baldwin, M. P., X. Cheng, and T. J. Dunkerton, 1994: Observed correlations between winter-mean tropospheric and stratospheric circulation anomalies. *Geophys. Res. Lett.*, **21**, 1141–1144.

Baldwin, M. P., D. B. Stephenson, and I. T. Jolliffe, 2009: Spatial weighting and iterative projection methods for EOFs. *J. Clim.*, **22**, 234–243.

Barnes, E. A., and D. L. Hartmann, 2010: Testing a theory for the effect of latitude on the persistence of eddy-driven jets using CMIP3 simulations. *Geophys. Res. Lett.*, **37**, L15 801.

Barnes, E. A., D. L. Hartmann, D. M. W. Frierson, and J. Kidston, 2010: Effect of latitude on the persistence of eddy-driven jets. *Geophys. Res. Lett.*, **37**, L11 804.

Benedict, J. J., S. Lee, and S. B. Feldstein, 2004: Synoptic view of the North Atlantic Oscillation. *J. Atmos. Sci.*, **61**, 121–144.

Butchart, N., and E. E. Remsberg, 1986: The area of the stratospheric polar vortex as a diagnostic for tracer transport on an isentropic surface. *J. Atmos. Sci.*, **43**, 1319–1339.

Chen, G., and P. Zurita-Gotor, 2008: The Tropospheric Jet Response to Prescribed Zonal Forcing in an Idealized Atmospheric Model. *J. Atmos. Sci.*, **65**, 2254–2271.

Chen, G., and R. A. Plumb, 2009: Quantifying the Eddy Feedback and the Persistence of the Zonal Index in an Idealized Atmospheric Model. *J. Atmos. Sci.*, **66**, 3707–3720.

DeWeaver, E., and S. Nigam, 2000: Do Stationary Waves Drive the Zonal-Mean Jet Anomalies of the Northern Winter? *J. Clim.*, **13**, 2160–2176.

Edmon Jr., H. J., B. J. Hoskins, and M. E. Mcintyre, 1980: Eliassen-Palm cross sections for the troposphere. *J. Atmos. Sci.*, **37**, 2600–2616.

Franzke, C., S. Lee, and S. B. Feldstein, 2004: Is the North Atlantic Oscillation a Breaking Wave? *J. Atmos. Sci.*, **61**, 145–160.

Fyfe, J. C., and O. a. Saenko, 2006: Simulated changes in the extratropical Southern Hemisphere winds and currents. *Geophys. Res. Lett.*, **33**, L06 701.

Gerber, E. P., and G. K. Vallis, 2007: Eddy-zonal flow interactions and the persistence of the zonal index. *J. Atmos. Sci.*, **64**, 3296–3311.

Haigh, J. D., M. Blackburn, and R. Day, 2005: The response of tropospheric circulation to perturbations in lower-strato- spheric temperature. *J. Climate*, **18**, 3672–3685.

Hartmann, D. L., 2007: The Atmospheric General Circulation and Its Variability. **85**, 123–143.

Hartmann, D. L., and F. Lo, 1998: Wave-driven zonal flow vacillation in the Southern Hemisphere. *J. Atmos. Sci.*, **55**, 1303–1315.

Hartmann, D. L., and P. Zuercher, 1998: Response of baroclinic life cycles to barotropic shear. *J. Atmos. Sci.*, **55**, 297–313.

Held, I. M., and M. Suarez, 1994: A proposal for the intercomparison of the dynamical cores of atmospheric general circulation models. *Bull. Am. Meteorol. Soc.*, **75**, 1825–1830.

Kidston, J., and G. K. Vallis, 2012: The Relationship between the Speed and the Latitude of an Eddy-Driven Jet in a Stirred Barotropic Model. *J. Atmos. Sci.*, **69**, 3251–3263.

Kutzbach, J. E., 1970: Large-scale features of monthly mean Northern Hemisphere anomaly maps of sea-level pressure. *Mon. Weather Rev.*, **98**, 708–716.

Limpasuvan, V., and D. L. Hartmann, 1999: Eddies and the annular modes of climate variability. *Geophys. Res. Lett.*, **26**, 3133–3136.

Lorenz, D. J., and D. L. Hartmann, 2001: Eddy-zonal flow feedback in the Southern Hemisphere. *J. Atmos. Sci.*, **58**, 3312–3327.

Lorezn, E. N., 1967: *The Nature and Theory of the General Circulation of the Atmosphere*. World Meteorological Organization, 161 pp.

Mcintyre, M. E., and T. N. Palmer, 1983: Breaking planetary waves in the stratosphere. *Nature*, **305**, 593–600.

Nakamura, N., and D. Zhu, 2010: Finite-Amplitude Wave Activity and Diffusive Flux of Potential Vorticity in Eddy–Mean Flow Interaction. *J. Atmos. Sci.*, **67**, 2701–2716.

Namias, J., 1950: The index cycle and its role in the general circulation. *J. Meteorol.*, **7**, 130–139.

Nigam, S., 1990: On the structure of variability of the observed tropospheric and stratospheric zonal-mean zonal wind. *J. Atmos. Sci.*, **47**, 1799–1813.

Rivière, G., 2009: Effect of Latitudinal Variations in Low-Level Baroclinicity on Eddy Life Cycles and Upper-Tropospheric Wave-Breaking Processes. *J. Atmos. Sci.*, **66**, 1569–1592.

Robinson, W. A., 2000: A Baroclinic Mechanism for the Eddy Feedback on the Zonal Index. *J. Atmos. Sci.*, **57**, 415–422.

Robinson, W. A., 2006: On the self-maintenance of midlatitude jets. *J. Atmos. Sci.*, **63**, 2109–2123.

Rogers, J. C., and H. van Loon, 1982: Spatial variability of sea level pressure and 500 mb height anomalies over the Southern Hemisphere. *Mon. Weather Rev.*, **110**, 1375–1392.

Rossby, C. G., 1939: Relation between variations in the intensity of the zonal circulation of the atmosphere and the displacements of the semi-permanent centers of action. *J. Mar. Res.*, 38–55.

Sardeshmukh, P. D., and B. J. Hoskins, 1988: The generation of global rotational flow by steady idealized tropical divergence. *J. Atmos. Sci.*, **45**, 1228–1251.

Simmons, A. J., and B. J. Hoskins, 1978: The life cycles of some nonlinear baroclinic waves. *J. Atmos. Sci.*, **35**, 414–432.

Simmons, A. J., and B. J. Hoskins, 1980: Barotropic influences on the growth and decay of nonlinear baroclinic waves. *J. Atmos. Sci.*, **37**, 1679–1684.

Simpson, I. R., M. Blackburn, and J. D. Haigh, 2012: A Mechanism for the Effect of Tropospheric Jet Structure on the Annular Mode–Like Response to Stratospheric Forcing. *J. Atmos. Sci.*, **69**, 2152–2170.

Simpson, I. R., T. G. Shepherd, P. Hitchcock, and J. F. Scinocca, 2013: Southern Annular Mode Dynamics in Observations and Models. Part II: Eddy Feedbacks. *J. Clim.*, **26**, 5220–5241.

Solomon, A., G. Chen, and J. Lu, 2012: Finite-amplitude Lagrangian-mean wave activity diagnostics applied to the baroclinic eddy life cycle. *J. Atmos. Sci.*, **69**, 3013–3027.

Thompson, D.W. J., and S. Solomon (2002), Interpretation of recent Southern Hemisphere climate change, *Science*, **296**, 895–899.

Thompson, D. W. J., and J. M. Wallace, 2000: Annular modes in the extratropical circulation. Part I: Month-to-month variability*. *J. Clim.*, **13**, 1000–1016.

Thompson, D. W. J., J. M. Wallace, and H. C. Gabriele, 2000: Annular Modes in the Extratropical Circulation . Part II : Trends *. *J. Clim.*, **13**, 1018–1037.

Thorncroft, C. D., and B. J. Hoskins, 1993: Two paradigms of baroclinic-wave life-cycle behaviour. *Q. J. R. Meteorol. Soc.*, **119**, 17–55.

Trenberth, K. E., 1979: Interannual variability of the 500 mb zonal mean flow in the Southern Hemisphere. *Mon. Weather Rev.*, **107**, 1515–1524.

Vallis, G. K., 2006: *Atmospheric and Oceanic Fluid Dynamics: Fundamentals and Large-scale Circulation*. Cambridge University Press, 745 pp.

Webster, P. J., and J. L. Keller, 1975: Atmospheric variations: Vacillations and index cycles. *J. Atmos. Sci.*, **32**, 1283–1300.

Willett, H. C., 1948: Patterns of world weather changes. *Trans. Amer. Geophys. Union*, **29**, 803–809

Zhang, Y., X.-Q. Yang, Y. Nie, and G. Chen, 2012: Annular Mode–Like Variation in a Multilayer Quasigeostrophic Model. *J. Atmos. Sci.*, **69**, 2940–2958.

Zurita-Gotor, Pablo, Javier Blanco-Fuentes, Edwin P. Gerber, 2014: The Impact of Baroclinic Eddy Feedback on the Persistence of Jet Variability in the Two-Layer Model. *J. Atmos. Sci.*, **71**, 410–429.

APPENDIX A

MODIFIED LAGRANGIAN-MEAN

A conceptual representation of the MLM is presented here. Figure 18 schematically depicts (5) above. It is a four-step process to calculate wave activity. Tracer contours are first calculated over the entire globe and are systematically examined to determine wave amplitude. Here, the tracer used is vorticity. Second, equivalent latitude is determined for each contour (Butchart and Remsberg 1984). A line of equivalent latitude is drawn that produces equal area bounded between equivalent latitude and contour to the south, red region, and north, blue region. This equal area-weighted scheme is analogous to a mass-weighted average based on each contour. Once these areas are determined, the eddy operator in (5) can be used which takes the difference between the vorticity integrated south of the equivalent latitude line from the vorticity integrated north of the equivalent latitude line is calculated. When supplying vorticity to (5), it provides an amplitude of the vorticity waves in ms^{-1}.

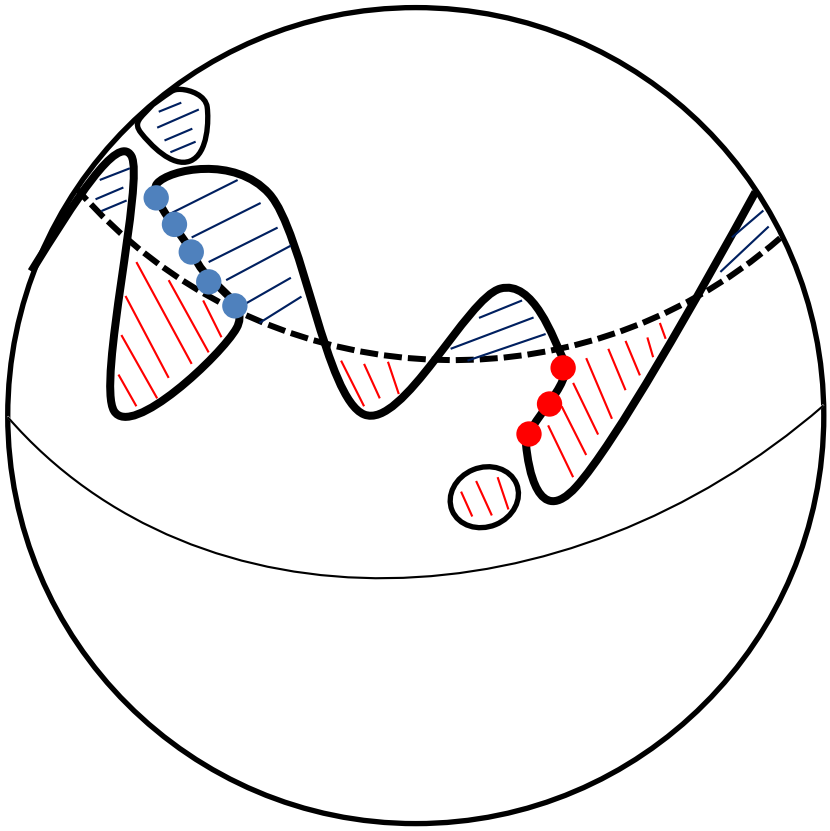

Figure 18: Schematic to conceptually use the eddy operator in (5). Thick line is a tracer contour of vorticity; thick dashed line is equivalent latitude; red and blue lines indicate area to the south and north of the equivalent latitude, respectively, and red and blue dots indicate AWB and CWB, respectively.

APPENDIX B

WAVE BREAKING

Wave breaking is calculated in a similar fashion to Riviere (2009) with a few other details. The Northern Hemisphere will be used as an example but can be extended easily into the Southern Hemisphere. First, vorticity needs to be calculated over the entire domain, QG PV and absolute vorticity are used in this study. Wave breaking is then calculated at each pressure level in the atmosphere. Once vorticity contours are calculated, only the contours that fully circumvent the globe are used to define wave breaking. Cut-off blobs of vorticity are excluded from actual breaking events. Each contour of vorticity is then systematically examined from lowest longitude and latitude to highest longitude and latitude. Since a single contour is being analyzed, constant vorticity, the actually longitude and latitude values are being scrutinized. Following a contour, longitude will continue to increase until a breaking event is discovered where longitude begins to decrease. From the first point at which breaking is found, if the latitude of the next point decreases, AWB is marked, or if the latitude of the next point increases, CWB is marked, see Fig. 18. In order to fully be classified as wave breaking, a few other criterions must be satisfied. There must be three points in a row classified as breaking to qualify. An entire contour of vorticity must either be AWB or CWB, not both. This second stipulation may cause issues in observations where contours become extremely complex, but in these models, it is sufficient. A wave breaking frequency can be calculated from the wave breaking events by simply adding the number of events for AWB and CWB to obtain maps of frequency.